Correlated model for quasi-elastic responses in finite nuclear systems

Giampaolo Co'

Dipartimento di Fisica, Università di Lecce and I.N.F.N. sez. di Lecce,
I-73100 Lecce, Italy

and

Antonio M. Lallena

Departamento de Física Moderna, Universidad de Granada,
E-18071 Granada, Spain

Abstract

A model to calculate nuclear responses considering short-range correlation effects is presented. The model is applied to the study of electromagnetic responses induced by one-body operators. We calculate one- and two-nucleon emission responses and cross sections of the ^{16}O and ^{40}Ca nuclei in the quasi-elastic region, and we compare them with experimental data.

PACS number(s): 21.10.Ft, 21.60.-n

1 Introduction

The study of atomic nuclei has been characterized in the last few years by the development and the application of technologies able to deal with realistic nuclear interactions. In the nuclear structure jargon one calls realistic those interactions whose parameters have been fixed to reproduce the properties of two, and eventually three, nucleon systems.

A large number of theories has been developed to tackle the problem of solving the Schrödinger equation with realistic interactions. Three or four nucleon systems are described with Faddeev [1, 2], Correlated Hyperspherical Harmonics Expansion [3, 4] and Green Function Monte Carlo [5] techniques which solve the Schrödinger equation without approximations. The Green Function Monte Carlo technique has also been applied, with great success, to nuclei up to A=7 [5].

Mainly for computational reasons, the straightforward applications of the above theories to heavier nuclear systems is not affordable, therefore different approaches like, Cluster Monte Carlo [6], Brueckner theory [7], Exponential S [8], Correlated Basis Function (CBF) [9], have been developed with the aim of obtaining approximate, but still accurate, solutions of the many-body Schrödinger equation.

Among these theories the CBF [10] has been well tested and widely applied in infinite nuclear systems like nuclear and neutron matter [11]-[13]. These studies have shown that, in the framework of the CBF theory, the Fermi Hypernetted Chain (FHNC) resummation technique with the Single Operator Chain (SOC) approximation provides solutions of the Schrödinger equation having accuracy of about 1 MeV per nucleon on the binding energy. In this computational scheme the use of Argonne nucleon-nucleon potentials [14, 15] together with Urbana three-body forces [16], provides equations of state whose minima are rather close to the empirical one. In the same framework also the nuclear matter responses to external probes have been calculated obtaining a satisfactory agreement with experimental inelastic electron scattering data [17, 18].

The success of the infinite nuclear matter results has induced to apply the CBF theory to the description of the ground state of finite nuclear systems. Recently, ^{16}O and ^{40}Ca ground states have been described within the FHNC-SOC computational scheme with interactions including tensor, spin-orbit terms and three-body forces [9].

In this paper we deal with the problem of describing excited states of finite nuclei within the CBF computational scheme. The model we present is inspired to the nuclear matter works of Refs. [17, 18]. While in these works the CBF cluster expansion has been fully considered, in our model we retain only those terms containing a single correlation function. The validity of this truncation has been tested, for the nuclear matter charge response, in Ref. [19]. Because of the excellent agreement between the full calculation and our truncated model we felt confident enough to extend our model the current operators.

Our model treats the Short Range Correlations (SRC) but does not consider collective nuclear excitations. For this reason we have applied it to the description of the nuclear responses in the quasi-elastic region where the collective effects are negligible [20, 21].

In this paper we shall deal only with inclusive electron scattering data, and we consider excited states with both one and two particles in the continuum. The two nucleon emission is treated as a genuine SRC effect, and we neglect the contribution of the two-body currents.

After briefly reviewing in section 2 the approach of Ref. [17], we present in section 3 our model, and we apply it in section 4 to inclusive electron scattering. The results obtained in the calculations of the ^{16}O and ^{40}Ca quasi-elastic responses are presented in section 5. In section 6 we summarize our work and we draw our conclusions.

2 Responses in a correlated theory

The linear response of a many-body system to the perturbations induced by an external operator $O(\mathbf{q})$ is given by:

$$S(\mathbf{q},\omega) \,=\, -\frac{1}{\pi}\,\mathrm{Im}\,\mathrm{D}(\mathbf{q},\omega)\,, \tag{1}$$

with

$$D(\mathbf{q},\omega) \,=\, \langle\widetilde{\Psi}_0 \,|\, O^+(\mathbf{q})\,(H - E_0 - \omega + i\eta)^{-1}\, O(\mathbf{q}) \,|\, \widetilde{\Psi}_0\rangle\,, \tag{2}$$

where we have indicated with $|\,\widetilde{\Psi}_n\rangle$ the normalized eigenstates of the nuclear hamiltonian H:

$$|\,\widetilde{\Psi}_n\rangle \,=\, \frac{|\Psi_n\rangle}{\langle\Psi_n|\Psi_n\rangle^{\frac{1}{2}}}\,. \tag{3}$$

In the previous equations $\mathbf{q}$ and ω represent the momentum and energy transferred to the nucleus.

Inserting in Eq. (2) a complete set of eigenvectors of H we obtain:

$$D(\mathbf{q},\omega) \,=\, \sum_n \frac{|\langle\widetilde{\Psi}_n \,|\, O(\mathbf{q}) \,|\, \widetilde{\Psi}_0\rangle|^2}{E_n - E_0 - \omega + i\eta} \,=\, \sum_n \xi_n^+(\mathbf{q})\,(E_n - E_0 - \omega + i\eta)^{-1}\,\xi_n(\mathbf{q})\,, \tag{4}$$

where we have defined:

$$\xi_n(\mathbf{q}) \,=\, \frac{\langle\Psi_n|\,O(\mathbf{q})\,|\Psi_0\rangle}{\langle\Psi_n|\Psi_n\rangle^{\frac{1}{2}}\,\langle\Psi_0|\Psi_0\rangle^{\frac{1}{2}}}\,. \tag{5}$$

Like in CBF theory we assume that the nuclear many-body ground state is described as a product of a correlation function G and a Slater determinant $|\Phi_0\rangle$ of a set of single particle wave functions occupying all, and only, the states below the Fermi surface:

$$|\Psi_0\rangle \,=\, G\,|\Phi_0\rangle\,. \tag{6}$$

Since the Slater determinant is already antisymmetrized with respect to the exchange of two nucleons, the correlation operator is given by a symmetrized product of two-body correlation operators:

$$G(1,2...A) \,=\, \mathcal{S}\left[\prod_{i<j} F_{ij}\right]\,, \tag{7}$$

where we have indicated with $\mathcal{S}$ the symmetrizer operator.

In modern nuclear structure calculations with realistic microscopic interactions, the two-body correlation operator is taken as a sum of operatorial dependent correlation functions

$$F_{ij} \,=\, \sum_{p=1,8} f^p(r_{ij})\,O^p_{ij}\,, \tag{8}$$

where the involved operators are:

$$O^{p=1,8}_{ij} \,=\, [1,\,\boldsymbol{\sigma}_i\cdot\boldsymbol{\sigma}_j,\,S_{ij},\,(\mathbf{L}\cdot\mathbf{S})_{ij}]\,\otimes\,[1,\,\boldsymbol{\tau}_i\cdot\boldsymbol{\tau}_j]\,, \tag{9}$$

with $S_{ij} = (3\,\hat{\mathbf{r}}_{ij}\cdot\boldsymbol{\sigma}_i\,\hat{\mathbf{r}}_{ij}\cdot\boldsymbol{\sigma}_j - \boldsymbol{\sigma}_i\cdot\boldsymbol{\sigma}_j)$ indicating the tensor operator, and $r_{ij} = |\mathbf{r}_i - \mathbf{r}_j|$ the distance between the positions of the particles i and j.

The ground state wave function is obtained by minimizing the ground state energy with respect to variations of the correlation function and of the single particle basis. In the theory developed in Ref. [17], the correlation operator G whose parameters have been fixed by the ground state minimization is used to generate the excited states of the system:

$$|\Psi_n\rangle \,=\, G\,|\Phi_n\rangle\,. \tag{10}$$

The mean-field excited states $|\Phi_n\rangle$ are obtained by making particle-hole excitations on $|\Phi_0\rangle$.

In order to use the cluster expansion techniques it is useful to rewrite the function $\xi_n(\mathbf{q})$ as:

$$\xi_n(\mathbf{q}) \,=\, \frac{\langle\Phi_n|\,G^+\,O(\mathbf{q})\,G|\Phi_0\rangle}{\langle\Phi_0|\,G^+\,G\,|\Phi_0\rangle}\left[\frac{\langle\Phi_0|\,G^+\,G\,|\Phi_0\rangle}{\langle\Phi_n|\,G^+\,G\,|\Phi_n\rangle}\right]^{\frac{1}{2}}\,. \tag{11}$$

The two factors in Eq. (11) are evaluated separately by expanding the numerator and the denominator in powers of the short-range function $F_{ij} - 1$ (see Ref. [17] for a detailed presentation of the cluster expansion of $\xi_n(\mathbf{q})$). In both factors the denominators cancel the unlinked diagrams.

3 The model

Our model simplifies the calculation of the cluster expansion of Eq. (11) by retaining only those terms involving a single correlation line. This model has been inspired by the results of Refs. [27, 28] where the density and momentum distributions of doubly closed shell nuclei, calculated with a single correlation line model, have been shown to be rather similar to those obtained with a complete CBF/FHNC calculations.

In the present article we consider that the external operator $O(\mathbf{q})$ is a one-body operator and we use only scalar correlations. Considering $O^p_{ij} = 0$ for $p > 1$ in Eq. (9), we can express the function $\xi_n(\mathbf{q})$ as:

$$\begin{aligned} \xi_n(\mathbf{q}) &= \frac{\langle \Phi_n | \prod_{i<j} f^+_{ij} \, O(\mathbf{q}) \prod_{i<j} f_{ij} \, |\Phi_0\rangle}{\langle \Phi_0 | \prod_{i<j} f^+_{ij} \prod_{i<j} f_{ij} \, |\Phi_0\rangle} \left[\frac{\langle \Phi_0 | \prod_{i<j} f^+_{ij} \prod_{i<j} f_{ij} \, |\Phi_0\rangle}{\langle \Phi_n | \prod_{i<j} f^+_{ij} \prod_{i<j} f_{ij} \, |\Phi_n\rangle} \right]^{\frac{1}{2}} \\ &= \frac{\langle \Phi_n | \, O(\mathbf{q}) \prod_{i<j} (1 + h_{ij}) \, |\Phi_0\rangle}{\langle \Phi_0 | \prod_{i<j} (1 + h_{ij}) \, |\Phi_0\rangle} \left[\frac{\langle \Phi_0 | \prod_{i<j} (1 + h_{ij}) \, |\Phi_0\rangle}{\langle \Phi_n | \prod_{i<j} (1 + h_{ij}) \, |\Phi_n\rangle} \right]^{\frac{1}{2}} , \end{aligned} \tag{12}$$

where we have considered that f_{ij} is a real scalar function, therefore commuting with the operator $O(\mathbf{q})$, and we have defined $h_{ij} = f^2_{ij} - 1$.

The approximation of our model consists in retaining in Eq.(12) only those diagrams having a single h function:

$$\xi_n(\mathbf{q}) \rightarrow \xi^1_n(\mathbf{q}) \; = \; \langle \Phi_n | \, O(\mathbf{q}) \sum_{i<j} (1 + h_{ij}) \, |\Phi_0\rangle_L \, , \tag{13}$$

where the subindex L indicates that only the linked diagrams are considered. This result has been obtained using the same procedure used in Ref. [27] for the density distribution. The first step consists in making the full cluster expansion of numerators and denominators, and this allows the elimination of the unlinked diagrams. Only at this point we truncate the obtained result by considering only the first order terms in h_{ij}.

The terms contributing to $\xi^1_n(\mathbf{q})$ are presented as Mayer like diagrams in Figs. 1 and 2 for 1p-1h and 2p-2h excitations respectively. In each diagram, the black square indicates the coordinate where the excitation one-body operator $O(\mathbf{q})$ is acting, while the black dots indicate the other coordinates. The dashed line indicates the correlation function h, which operates on two-coordinates only, and the continuous oriented lines indicate the single particle wave functions ϕ. We have used the convection of considering entering into a point the wave functions of the state $|\Phi\rangle$, while the wave functions of the state $\langle\Phi|$ are exiting from the point. The letters i, j, k indicate single particle wave functions below the Fermi surface and imply a summation over them. With p and h we have labelled those particle and hole states whose quantum numbers characterize the full many-body excited state.

Let's first consider the case when the nuclear final states have only one particle in the continuum. If we label with 1 the coordinate where the external operator $O(\mathbf{q})$ is acting, we can specify the ξ^1 in Eq. (13) as:

$$\begin{aligned} \xi^1_{\rm 1p1h}(\mathbf{q}) \;\; &= \;\; \langle \Phi_{\rm 1p1h} | \, O(\mathbf{q}) \, |\Phi_0\rangle \, + \, \langle \Phi_{\rm 1p1h} | \, O(\mathbf{q}) \sum_{j>1}^{A} h_{1j} \, |\Phi_0\rangle \\ & \quad + \langle \Phi_{\rm 1p1h} | \, O(\mathbf{q}) \sum_{1<i<j}^{A} h_{ij} \, |\Phi_0\rangle \, . \end{aligned} \tag{14}$$

The above expression shows that our model, in addition to the uncorrelated transitions represented by the the one-point diagram (1.1) in Fig. 1, generates also two- and three-point diagrams. The presence of both two- and three-point diagrams is necessary to have a correct normalization of the many body wave function. This can be seen by considering that, if $O(\mathbf{q})$ is the density operator, in the limit for $q \rightarrow 0$, when $p = h$, the sum on all the hole single particle wave functions should provide the proper number of nucleons A, as it happens in Refs. [27, 28]. In this limit, the diagrams containing a correlation line should not contribute. This can be seen in Fig. 1, by joining the p and h lines and considering that in the three-point diagrams the $q \to 0$ limit implies that the wave functions linked to the black square should be equal because of the orthonormality of the set of single particle wave functions. One can then observe that the contribution of the (2.1) and (2.3) diagrams is exactly canceled by that of the (3.2), (3.4) and (3.6) diagrams, and the contribution of the (2.2) and (2.4) diagrams is canceled by that of the (3.1), (3.3) and (3.5) diagrams.

When the nuclear final state is characterized by two-particle two-hole excitations, the function $\xi^1_n(\mathbf{q})$ is given by:

$$\xi^1_{\rm 2p2h}(\mathbf{q}) \,=\, \langle \Phi_{\rm 2p2h}|\, O(\mathbf{q}) \sum_{1<j}^{A} h_{1j} \,|\Phi_0\rangle \,+\, \langle \Phi_{\rm 2p2h}| O(\,\mathbf{q}) \sum_{1<i<j}^{A} h_{ij} \,|\Phi_0\rangle \,. \tag{15}$$

As expected, the uncorrelated term does not appear, since a one-body operator cannot lead to a 2p-2h final state. The 4 two-point diagrams and the 12 three-point diagrams we consider are shown in Fig. 2. Also in this case the set of diagrams conserves the proper normalization. In analogy with the discussion done for the 1p-1h case one can see that, in the limit $q \to 0$ and setting $p_1 = h_1$ and $p_2 = h_2$ the contribution of the diagrams of Fig. 2 is zero, as expected.

4 Electro-magnetic excitations

The response model presented in the previous sections has been applied to the description of inclusive electron scattering processes considering both one- and two- nucleon emission.

In Plane Wave Born Approximation, the inclusive electron scattering cross section can be written as:

$$\begin{aligned} \frac{{\rm d}^2\sigma}{{\rm d}\Omega'{\rm d}\epsilon'} \quad &= \quad \sigma_M \left\{ \frac{q^4_\mu}{\mathbf{q}^4} \left[R^{\rm 1p1h}_L(q,\omega) + R^{\rm 2p2h}_L(q,\omega) \right] \right. \\ &\left. + \left(\tan^2 \frac{\theta}{2} - \frac{q^2_\mu}{2\mathbf{q}^2} \right) \left[R^{\rm 1p1h}_T(q,\omega) + R^{\rm 2p2h}_T(q,\omega) \right] \right\} \,, \end{aligned} \tag{16}$$

where θ is the scattering angle, q^μ the four-momentum transfer verifying the relation $q^2_\mu = \omega^2 - \mathbf{q}^2$, and σ_M is the Mott cross section:

$$\sigma_M = \left(\frac{\alpha \cos(\theta/2)}{2\epsilon_i \sin^2(\theta/2)} \right)^2 \,. \tag{17}$$

In the last equation α is the fine structure constant and ϵ_i is the initial energy of the electron.

The electromagnetic responses R_L and R_T, depending from $q \equiv |\mathbf{q}|$ and ω, are obtained by evaluating the responses $S(\mathbf{q},\omega)$ in Eq. (1) for charge and current operators respectively, and multiplying them by the electromagnetic nucleon form factors. In Eq. (16) the 1p-1h and 2p-2h responses do not interfere with each other because they produce two different final states.

We have calculated the longitudinal responses using the charge operator:

$$O(\mathbf{q}) \,\to\, \rho(\mathbf{q}) \,=\, \int {\rm d}^3r \; e^{i\mathbf{q}\cdot\mathbf{r}} \, \rho(\mathbf{r}) \,, \tag{18}$$

with

$$\rho(\mathbf{r}) \,=\, \sum_{k=1}^{A} \frac{1+\tau_3(k)}{2} \, \delta(\mathbf{r}-\mathbf{r}_k) \,, \tag{19}$$

where $\tau_3(k)$ is the third component of the isospin of the k-th nucleon.

The transverse responses have been calculated considering convection and magnetization currents:

$$O(\mathbf{q}) \,\to\, \mathbf{J}(\mathbf{q}) = \mathbf{j}^c(\mathbf{q}) + \mathbf{j}^m(\mathbf{q}) = \int {\rm d}^3r \; e^{i\mathbf{q}\cdot\mathbf{r}} \left[\mathbf{j}^c(\mathbf{r}) + \mathbf{j}^m(\mathbf{r}) \right], \tag{20}$$

with

$$\mathbf{j}^c(\mathbf{r}) \,=\, \sum_{k=1}^{A} \frac{1}{i2M_k} \frac{1+\tau_3(k)}{2} \left[\delta(\mathbf{r}-\mathbf{r}_k)\,\nabla_k \,+\, \nabla_k\,\delta(\mathbf{r}-\mathbf{r}_k)\right], \tag{21}$$

and

$$\mathbf{j}^m(\mathbf{r}) \,=\, \sum_{k=1}^{A} \frac{1}{M_k} \left(\mu_P \frac{1+\tau_3(k)}{2} + \mu_N \frac{1-\tau_3(k)}{2}\right) \nabla_k \times \delta(\mathbf{r}-\mathbf{r}_k)\,\boldsymbol{\sigma}(k)\,. \tag{22}$$

In the above equation we have indicated with M_k and $\boldsymbol{\sigma}(k)$ the mass and Pauli spin matrices corresponding to the k-th nucleon, and with μ_P (μ_N) the proton (neutron) anomalous magnetic moment.

Since in the quasi-elastic peak the contribution of $\mathbf{j}^c$ is small as compared to that of $\mathbf{j}^m$ (see the discussion of Fig. 5 in the next section) we have considered the convection current only in the uncorrelated one-body term (1.1) of Fig. 1.

We restrict our study to the investigation of doubly closed shell nuclei and we suppose that the target nucleus makes a transition from its ground state to an excited state characterized by the total angular momentum J, its projection M on the quantization axis, and the parity $\Pi = \pm 1$. The responses can be written as:

$$R_L(q,\omega) \,=\, \sum_{J,M}^{\infty} |\langle \Psi^{\Pi}_{JM}|\, M_{JM}(q)\, |\Psi^1_{00}\rangle|^2\, \delta(E_J - E_0 - \omega) \tag{23}$$

and

$$R_T(q,\omega) \,=\, \sum_{J,M}^{\infty} \left\{ |\langle \Psi^{\Pi}_{JM}|\, T^{\mathrm{E}}_{JM}(q)\, |\Psi^1_{00}\rangle|^2 \,+\, |\langle \Psi^{\Pi}_{JM}|\, T^{\mathrm{M}}_{JM}(q)\, |\Psi^1_{00}\rangle|^2 \right\} \delta(E_J - E_0 - \omega)\,, \tag{24}$$

where we have not indicated the parity of the ground state which is always positive in our case. The M_{JM} and T_{JM} operators used in the previous equations are obtained by making a multipole expansion of Eqs. (18) and (20). For the charge we have:

$$M_{JM}(q) \,=\, \int \mathrm{d}^3 r\, j_J(qr)\, Y_{JM}(\hat{\mathbf{r}})\, \rho(\mathbf{r})\,, \tag{25}$$

where we have indicated with $\hat{\mathbf{r}}$ the θ and ϕ angles characterizing the vector $\mathbf{r}$ in polar coordinates, with Y_{JM} the spherical harmonics and with j_J the spherical Bessel functions.

For the current we should distinguish between the electric excitations (E) with natural parity $\Pi = (-1)^J$ and the magnetic excitations (M) with unnatural parity $\Pi = (-1)^{J+1}$:

$$T^{\mathrm{E}}_{JM}(q) \,=\, \frac{1}{q} \int \mathrm{d}^3 r\, \left\{ \nabla \times \left[j_J(qr)\, \mathbf{Y}^M_{JJ}(\hat{\mathbf{r}}) \right] \right\} \cdot \mathbf{J}(\mathbf{r}) \tag{26}$$

and

$$T^{\mathrm{M}}_{JM}(q) \,=\, \int \mathrm{d}^3 r\, j_J(qr)\, \mathbf{Y}^M_{JJ}(\hat{\mathbf{r}}) \cdot \mathbf{J}(\mathbf{r})\,. \tag{27}$$

where we have used the symbol $\mathbf{Y}^M_{JJ}$ to indicate the vector spherical harmonics [22].

We calculate the responses using the expressions (1), (4) and (13), and we rewrite Eqs. (23) and (24) as:

$$R_L(q,\omega) \,=\, 4\pi \sum_{J}^{\infty} |\langle \Phi^{\Pi}_J \|\, M_J(q) \sum_{i<j} (1 + h_{ij})\, \|\Phi^1_0\rangle|^2\, \delta(E_J - E_0 - \omega) \tag{28}$$

and

$$\begin{aligned} R_T(q,\omega) \quad &= \quad 4\pi \sum_{J}^{\infty} \Bigg\{ |\langle \Phi^{\Pi}_J \|\, T^{\mathrm{E}}_J(q) \sum_{i<j} (1 + h_{ij})\, \|\Phi^1_0\rangle|^2 \\ &\qquad + |\langle \Phi^{\Pi}_J \|\, T^{\mathrm{M}}_{JM}(q) \sum_{i<j} (1 + h_{ij})\, \|\Phi^1_0\rangle|^2 \Bigg\}\, \delta(E_J - E_0 - \omega)\,. \end{aligned} \tag{29}$$

The above expressions have been obtained by applying the Wigner-Eckart theorem, therefore the symbol " $\|$ " indicates that the angular part should be calculated by considering only the reduced matrix elements.

The calculations of the transition matrix elements are carried out by performing a multipole expansion of the correlation function h:

$$h_{ij} \;=\; h(r_{ij}) \;=\; h(r_i, r_j, \cos\theta_{ij}) \;=\; \sum_{L=0}^{\infty} h_L(r_i, r_j)\, P_L(\cos\theta_{ij})\,, \tag{30}$$

where P_L are the associated Legendre polynomials. Because of the completeness and the orthogonality of the Legendre polynomials, the $h_L(r_i, r_j)$ terms can be evaluated as:

$$h_L(r_i, r_j) \;=\; \frac{2L+1}{2} \int_{-1}^{1} \mathrm{d}(\cos\theta_{ij})\, P_L(\cos\theta_{ij})\, h(r_i, r_j, \cos\theta_{ij})\,. \tag{31}$$

Eqs. (28) and (29) show that the final state quantum numbers are determined by the quantum numbers of the uncorrelated many body state $|\Phi^{\Pi}_{JM}\rangle$ which is built as a Slater determinant of single particle wave functions of the form:

$$\phi_k(\mathbf{r}) \;\equiv\; R^t_{nlj}(r) \sum_{\mu s} \langle l\mu \frac{1}{2} s | jm\rangle\, Y_{l\mu}(\hat{\mathbf{r}})\, \chi_s\, \chi_t\,, \tag{32}$$

where χ_s and χ_t are the spin and isospin wave functions respectively and $\langle l\mu\frac{1}{2}s|jm\rangle$ a Clebsh-Gordan coefficient.

We treat now separately the one and two nucleon emission cases. In the first one, once the hole is fixed, energy conservation defines the value of the emitted particle energy: $\epsilon_p = \omega + \epsilon_h$. The angular momentum coupled Slater determinant is related to the uncoupled one by the relation:

$$|\Phi^{\Pi}_{JM}(\mathrm{1p1h})\rangle \;=\; \sum_{\mathrm{m_p m_h}} (-1)^{\mathrm{j_h - m_h}}\, \langle \mathrm{j_p m_p j_h - m_h | JM}\rangle\, |\Phi^{\Pi}_{\mathrm{1p1h}}\rangle\,, \tag{33}$$

where j_p and j_h are the particle and hole angular momenta and m_p and m_h their third components. We insert the expression (33) into Eq. (14) and apply the Wigner-Eckart theorem. Using the orthornormality of the single particle wave functions we obtain the following expression:

$$\xi^{1,J}_{\mathrm{1p1h}}(\mathbf{q}) \;=\; \langle p \|\, O_J(\mathbf{q})\, \| h\rangle \;+\; \sum_{j}^{A} \langle pj \|\, O_J(\mathbf{q})\, h_{12}\, \| hj\rangle \;+\; \sum_{j,k}^{A} \langle pjk \|\, O_J(\mathbf{q})\, h_{23} \| hjk\rangle\,. \tag{34}$$

In this equation we have labelled with 1 the coordinate where the electromagnetic one-body operator is acting. The second and the third terms of Eq. (34) produce the two- and three-point diagrams of Fig. 1 respectively.

The multipole expanded expression of a generic one-body operator is formed by the product of a term depending on q and $\mathbf{r}_1$ multiplied by a term depending only on the angular coordinates:

$$O_{JM}(\mathbf{q}) = F_J(qr_1) O_{JM}(\hat{\mathbf{r}}_1). \tag{35}$$

In the case we are interested this is obtained by inserting the expressions (19), (21) and (22) into Eqs. (25), (26) and (27).

We present in the following the expressions of the terms of Eq. (34) using the notation of Ref. [22] to indicate the 3j, 6j and 9j symbols of Wigner. For the one-point diagram we obtain:

$$D^{(\mathrm{1p1h})}_1 \;=\; \omega^J_{ph} \int \mathrm{d}r_1\, r_1^2\, R^*_p(r_1)\, F_J(qr_1)\, R_h(r_1)\,, \tag{36}$$

where we have defined:

$$\omega^K_{\alpha\beta} = \langle l_\alpha \frac{1}{2} j_\alpha \parallel O_K(\hat{\mathbf{r}}_1) \parallel l_\beta \frac{1}{2} j_\beta \rangle \tag{37}$$

The expressions we have obtained for the two-point diagrams are:

$$D^{(\mathrm{1p1h})}_{2.1} = 4\pi\, \omega^J_{ph} \int \mathrm{d}r_1\, r_1^2\, R^*_p(r_1)\, F_J(qr_1)\, R_h(r_1)\, \mathcal{H}^{[\rho]}_0(r_1)\,, \tag{38}$$

$$\begin{aligned} D^{(\mathrm{1p1h})}_{2.2} &= 4\pi\, (-1)^{j_p+j_h+J} \sum_{iLK} \delta_{t_i,t_h}\, (-1)^L\, \frac{\widehat{K}}{\widehat{L}^2}\, \gamma^L_{ih} \left\{ \begin{array}{ccc} L & K & J \\ j_p & j_h & j_i \end{array} \right\} \\ & \quad \omega^{LJ;K}_{pi} \int \mathrm{d}r_1\, r_1^2\, R^*_p(r_1)\, F_J(qr_1) R_i(r_1)\, \mathcal{H}^{[ih]}_L(r_1)\,, \end{aligned} \tag{39}$$

$$\begin{aligned} D^{(\mathrm{1p1h})}_{2.3} &= 4\pi\, \delta_{t_p,t_h}\, (-1)^J\, \frac{1}{\widehat{J}^3}\, \gamma^J_{ph} \sum_i \widehat{j}_i\, \omega^{JJ;0}_{ii} \\ & \quad \int \mathrm{d}r_1\, r_1^2\, R^*_i(r_1)\, F_J(qr_1) R_i(r_1)\, \mathcal{H}^{[ph]}_J(r_1)\,, \end{aligned} \tag{40}$$

$$\begin{aligned} D^{(\mathrm{1p1h})}_{2.4} &= 4\pi\, (-1)^{j_p+j_h} \sum_{iLK} \delta_{t_i,t_p}\, (-1)^K\, \frac{\widehat{K}}{\widehat{L}^2}\, \gamma^L_{pi} \left\{ \begin{array}{ccc} L & K & J \\ j_h & j_p & j_i \end{array} \right\} \\ & \quad \omega^{LJ;K}_{ih} \int \mathrm{d}r_1\, r_1^2\, R^*_i(r_1)\, F_J(qr_1)\, R_h(r_1)\, \mathcal{H}^{[pi]}_L(r_1)\,. \end{aligned} \tag{41}$$

In the previous equations, we have used the notation $\widehat{\alpha} = \sqrt{2\alpha+1}$ and the following definition of $\gamma^\lambda_{\alpha\beta}$:

$$\begin{aligned} \gamma^\lambda_{\alpha\beta} &= \langle l_\alpha \frac{1}{2} j_\alpha \parallel Y_\lambda(\hat{\mathbf{r}}) \parallel l_\beta \frac{1}{2} j_\beta \rangle \\ &= \frac{1}{\sqrt{4\pi}}\, (-1)^{j_\beta+\lambda-\frac{1}{2}}\, \xi(l_\alpha + l_\beta + \lambda)\, \widehat{j}_\alpha \widehat{j}_\beta \widehat{\lambda} \left(\begin{array}{ccc} j_\alpha & j_\beta & \lambda \\ \frac{1}{2} & -\frac{1}{2} & 0 \end{array} \right)\,, \end{aligned} \tag{42}$$

with $\xi(\alpha)$=1 if α is even and $\xi(\alpha)$=0 otherwise. The other symbols used are:

$$\omega^{LJ;K}_{\alpha\beta} = \langle \alpha \|\, [Y_L(\theta_1,\phi_1) \otimes O_J(1)]^K \, \|\beta\rangle\,, \tag{43}$$

and the integrals,

$$\mathcal{H}^{[\alpha\beta]}_L(r_1) = \int \mathrm{d}r_2\, r_2^2\, R^*_\alpha(r_2)\, h_L(r_1,r_2)\, R_\beta(r_2) \tag{44}$$

and, in Eq. (38),

$$\mathcal{H}^{[\rho]}_0 = \frac{1}{4\pi} \sum_i \widehat{j}_i^2\, \mathcal{H}^{ii}_0(r_1) = \int \mathrm{d}r_2\, r_2^2\, h_0(r_1,r_2)\, \rho(r_2)\,, \tag{45}$$

where

$$\rho(r) = \frac{1}{4\pi} \sum_i \widehat{j}_i^2\, |R_i(r)|^2 \tag{46}$$

is the nuclear density.

For the three-point diagrams we have obtained the following expressions:

$$D^{(\mathrm{1p1h})}_{3.1} = \sum_{ikL} \delta_{t_k,t_p}\, \delta_{t_i,t_p}\, \delta_{j_i,j_p}\, \xi(l_p + l_k + L)\, \xi(l_p + l_i)\, \widehat{j}_k^2 \left(\begin{array}{ccc} j_p & j_k & L \\ \frac{1}{2} & -\frac{1}{2} & 0 \end{array} \right)^2 \tag{47}$$

$$\omega_{ih}^{J} \int {\rm d}r_1\, r_1^2\, R_i^*(r_1)\, F_J(qr_1)\, R_h(r_1) \mathcal{J}_L^{[pk];[ki]}\,,$$

$$D_{3.2}^{(1p1h)} = 4\pi \sum_i \delta_{t_i,t_p}\, \delta_{j_i,j_p}\, \xi(l_p+l_i)\, \omega_{ih}^{J} \int {\rm d}r_1\, r_1^2\, R_i^*(r_1)\, F_J(qr_1)\, R_h(r_1) \mathcal{J}_0^{[pi];[\rho]}\,, \tag{48}$$

$$D_{3.3}^{(1p1h)} = \sum_{ikL} \delta_{t_i,t_h}\, \delta_{t_k,t_h}\, \delta_{j_k,j_h}\, \xi(l_i+l_h+L)\, \xi(l_k+l_h)\, \widehat{j}_i^2 \begin{pmatrix} j_i & j_h & L \\ \frac{1}{2} & -\frac{1}{2} & 0 \end{pmatrix}^2 \tag{49}$$
$$\omega_{pk}^{J} \int {\rm d}r_1\, r_1^2\, R_p^*(r_1)\, F_J(qr_1)\, R_k(r_1) \mathcal{J}_L^{[ih];[ki]}\,,$$

$$D_{3.4}^{(1p1h)} = 4\pi \sum_i \delta_{t_i,t_h}\, \delta_{j_i,j_h}\, \xi(l_i+l_h)\, \omega_{pi}^{J} \int {\rm d}r_1\, r_1^2\, R_p^*(r_1)\, F_J(qr_1)\, R_i(r_1) \mathcal{J}_0^{[ih];[\rho]}\,, \tag{50}$$

$$D_{3.5}^{(1p1h)} = 4\pi\, (-1)^J \sum_{ikL} \delta_{t_i,t_p}\, \delta_{t_k,t_h}\, (-1)^{j_i+j_k+L}\, \frac{1}{\widehat{L}^2}\, \gamma_{pi}^{L}\, \gamma_{kh}^{L} \begin{Bmatrix} j_p & j_h & J \\ j_k & j_i & L \end{Bmatrix} \tag{51}$$
$$\omega_{ik}^{J} \int {\rm d}r_1\, r_1^2\, R_i^*(r_1)\, F_J(qr_1)\, R_k(r_1) \mathcal{J}_L^{[pi];[kh]}\,,$$

$$D_{3.6}^{(1p1h)} = 4\pi\, \delta_{t_p,t_h}\, \gamma_{ph}^{J}\, \frac{1}{\widehat{J}^4} \sum_{ik} \delta_{t_i,t_k}\, \gamma_{ik}^{J}\, \omega_{ik}^{J} \int {\rm d}r_1\, r_1^2\, R_i^*(r_1)\, F_J(qr_1)\, \mathcal{J}_J^{[ph];[ki]}\,. \tag{52}$$

In these equations we have introduced the symbols:

$$\mathcal{J}_L^{[\alpha\beta];[\gamma\delta]} = \int {\rm d}r_1\, r_1^2\, R_\alpha^*(r_1)\, R_\beta(r_1)\, \mathcal{H}_L^{[\gamma\delta]}(r_1) \tag{53}$$

and

$$\mathcal{J}_0^{[\alpha\beta];[\rho]} = \int {\rm d}r_1\, r_1^2\, R_\alpha^*(r_1)\, R_\beta(r_1)\, \mathcal{H}_0^{[\rho]}(r_1)\,. \tag{54}$$

The equations presented above have been obtained for a generic one-body transition operator of the form of Eq. (35). The calculation of the electromagnetic response functions continues by inserting in the above equations the explicit expression of the charge and current operators, Eqs. (25)-(27). The final expressions are given in Appendix A.

In the case of two nucleon emission the total angular momentum and parity of the nuclear final state are given by the combination of the four angular momenta and the parities of the particle and hole states involved in the excitation. We have chosen to couple the angular momenta of the two hole states and of the two particle states first, and then, with another recoupling, to obtain the total angular momentum of the 2p-2h excited state:

$$|\Phi_{JM}^{\Pi}(2p2h)\rangle = \sum_{M_p,M_h} \langle J_p M_p J_h - M_h | JM\rangle \sum_{j_{p_1} m_{p_1} j_{p_2} m_{p_2}} \langle j_{p_1} m_{p_1} j_{p_2} m_{p_2} | J_p M_p\rangle$$
$$\sum_{j_{h_1} m_{h_1} j_{h_2} m_{h_2}} (-1)^{j_{h_1}+j_{h_2}-m_{h_1}-m_{h_2}} \langle j_{h_1} - m_{h_1} j_{h_2} - m_{h_2} | J_h M_h\rangle\, |\Phi_{2p2h}^{\Pi}\rangle \tag{55}$$

Inserting Eq. (55) into Eq. (15) and applying the Wigner-Eckart theorem we obtain the following expression:

$$\xi_{2p2h}^{1,J}(\mathbf{q}) = \langle p_1 p_2 \|\, O_J(\mathbf{q})\, h_{12}\, \| h_1 h_2\rangle + \sum_k^A \langle p_1 p_2 k \|\, O_J(\mathbf{q})\, h_{23}\, | h_1 h_2 k\rangle\,, \tag{56}$$

where the coordinate labels have the same meaning as in Eq. (34). In the 2p-2h excitation the energy conservation does not uniquely define the energies of the emitted particles since

$$\omega \,=\, \epsilon_{p_1} \,+\, \epsilon_{p_2} \,-\, \epsilon_{h_1} \,-\, \epsilon_{h_2}\,, \tag{57}$$

for this reason in Eq. (55) an integration on the energy of the particle p_2 is implied.

It is evident from Fig. 2 that the various diagrams can be related one to the other by changing the labels of the hole and of the particle states involved. We use the following symmetry relations to calculate the contribution of the various diagrams to the response:

$$\begin{aligned}
D^{(2\mathrm{p}2\mathrm{h})}_{2.2}[p_1h_1p_2h_2] &= (-1)^{j_{h_1}+j_{h_2}+J_h}\, D^{(2\mathrm{p}2\mathrm{h})}_{2.1}[p_1h_2p_2h_1]\,, \\
D^{(2\mathrm{p}2\mathrm{h})}_{2.3}[p_1h_1p_2h_2] &= (-1)^{j_{p_1}+j_{p_2}+J_p}\, D^{(2\mathrm{p}2\mathrm{h})}_{2.1}[p_2h_1p_1h_2]\,, \\
D^{(2\mathrm{p}2\mathrm{h})}_{2.4}[p_1h_1p_2h_2] &= (-1)^{j_{p_1}+j_{p_2}+J_p}\,(-1)^{j_{h_1}+j_{h_2}+J_h}\, D^{(2\mathrm{p}2\mathrm{h})}_{2.1}[p_2h_2p_1h_1].
\end{aligned} \tag{58}$$

The explicit expression of $D^{(2\mathrm{p}2\mathrm{h})}_{2.1}$ matrix element for a generic one-body operator is given by:

$$\begin{aligned}
D^{(2\mathrm{p}2\mathrm{h})}_{2.1}[p_1h_1p_2h_2] &= 4\pi\, \delta_{t_{p_2},t_{h_2}}\, \widehat{J}_p\, \widehat{J}_h \sum_{LK} (-1)^L\, \frac{\widehat{K}}{\widehat{L}^2}\, \gamma^L_{p_2h_2} \left\{ \begin{array}{ccc} j_{p_1} & j_{h_1} & K \\ j_{p_2} & j_{h_2} & L \\ J_p & J_h & J \end{array} \right\} \\
&\quad \int \mathrm{d}r_1\, r_1^2\, R^*_{p_1}(r_1)\, \omega^{LJ;K}_{p_1h_1}\, R_{h_1}(r_1)\, \mathcal{H}^{[p_2h_2]}_L(r_1)\,.
\end{aligned} \tag{59}$$

The symmetry relations we used to evaluate the the three-point diagrams are:

$$\begin{aligned}
D^{(2\mathrm{p}2\mathrm{h})}_{3.2}[p_1h_1p_2h_2] &= (-1)^{j_{h_1}+j_{h_2}+J_h}\, D^{(2\mathrm{p}2\mathrm{h})}_{3.1}[p_1h_2p_2h_1]\,, \\
D^{(2\mathrm{p}2\mathrm{h})}_{3.3}[p_1h_1p_2h_2] &= (-1)^{j_{p_1}+j_{p_2}+J_p}\, D^{(2\mathrm{p}2\mathrm{h})}_{3.1}[p_2h_1p_1h_2]\,, \\
D^{(2\mathrm{p}2\mathrm{h})}_{3.4}[p_1h_1p_2h_2] &= (-1)^{j_{p_1}+j_{p_2}+J_p}\,(-1)^{j_{h_1}+j_{h_2}+J_h}\, D^{(2\mathrm{p}2\mathrm{h})}_{3.1}[p_2h_2p_1h_1] \\
D^{(2\mathrm{p}2\mathrm{h})}_{3.6}[p_1h_1p_2h_2] &= (-1)^{j_{h_1}+j_{h_2}+J_h}\, D^{(2\mathrm{p}2\mathrm{h})}_{3.5}[p_1h_2p_2h_1]\,, \\
D^{(2\mathrm{p}2\mathrm{h})}_{3.7}[p_1h_1p_2h_2] &= (-1)^{j_{p_1}+j_{p_2}+J_p}\, D^{(2\mathrm{p}2\mathrm{h})}_{3.5}[p_2h_1p_1h_2]\,, \\
D^{(2\mathrm{p}2\mathrm{h})}_{3.8}[p_1h_1p_2h_2] &= (-1)^{j_{p_1}+j_{p_2}+J_p}\,(-1)^{j_{h_1}+j_{h_2}+J_h}\, D^{(2\mathrm{p}2\mathrm{h})}_{3.5}[p_2h_2p_1h_1]\,, \\
D^{(2\mathrm{p}2\mathrm{h})}_{3.10}[p_1h_1p_2h_2] &= (-1)^{j_{p_1}+j_{p_2}+J_p}\,(-1)^{j_{h_1}+j_{h_2}+J_h}\, D^{(2\mathrm{p}2\mathrm{h})}_{3.9}[p_2h_2p_1h_1]\,, \\
D^{(2\mathrm{p}2\mathrm{h})}_{3.12}[p_1h_1p_2h_2] &= (-1)^{j_{p_1}+j_{p_2}+J_p}\,(-1)^{j_{h_1}+j_{h_2}+J_h}\, D^{(2\mathrm{p}2\mathrm{h})}_{3.11}[p_2h_2p_1h_1]\,.
\end{aligned} \tag{60}$$

The corresponding matrix elements for a generic one-body operator are:

$$\begin{aligned}
D^{(2\mathrm{p}2\mathrm{h})}_{3.1}[p_1h_1p_2h_2] &= 4\pi\, \delta_{t_{p_2},t_{h_2}}\, (-1)^{j_{p_1}+j_{h_1}+J+1}\, \widehat{J}_p\, \widehat{J}_h \sum_{iL} \delta_{t_i,t_{h_1}}\, \frac{1}{\widehat{L}^2}\, \gamma^L_{p_2h_2}\, \gamma^L_{ih_1} \\
&\left\{ \begin{array}{ccc} j_{p_2} & J_h & j_i \\ j_{h_1} & L & j_{h_2} \end{array} \right\} \left\{ \begin{array}{ccc} J_p & J_h & J \\ j_i & j_{p_1} & j_{p_2} \end{array} \right\} \int \mathrm{d}r_1\, r_1^2\, R^*_{p_1}(r_1)\, \omega^J_{p_1i}\, R_i(r_1)\, \mathcal{J}^{[p_2h_2];[ih_1]}_L\,,
\end{aligned} \tag{61}$$

$$\begin{aligned}
D^{(2\mathrm{p}2\mathrm{h})}_{3.5}[p_1h_1p_2h_2] &= 4\pi\, \delta_{t_{p_1},t_{h_1}}\, (-1)^{j_{p_2}+j_{h_2}+J+1}\, \widehat{J}_p\, \widehat{J}_h \sum_{iL} \delta_{t_i,t_{p_2}}\, \frac{1}{\widehat{L}^2}\, \gamma^L_{p_1h_1}\, \gamma^L_{p_2i} \\
&\left\{ \begin{array}{ccc} j_i & j_{h_1} & J_p \\ j_{p_1} & j_{p_2} & L \end{array} \right\} \left\{ \begin{array}{ccc} J_p & J_h & J \\ j_{h_2} & j_i & j_{h_1} \end{array} \right\} \int \mathrm{d}r_1\, r_1^2\, R^*_i(r_1)\, \omega^J_{ih_2}\, R_{h_2}(r_1)\, \mathcal{J}^{[p_1h_1];[p_2i]}_L\,,
\end{aligned} \tag{62}$$

$$D^{(2\mathrm{p}2\mathrm{h})}_{3.9}[p_1h_1p_2h_2] = 4\pi\, \delta_{t_{p_2},t_{h_1}}\, \delta_{j_{p_2},j_{h_1}}\, (-1)^{j_{p_1}+j_{p_2}+j_{h_2}+J-\frac{1}{2}}\, \frac{\widehat{J}_p\, \widehat{J}_h}{\widehat{j}^2_{p_2}} \left\{ \begin{array}{ccc} J_p & J_h & J \\ j_{h_2} & j_{p_1} & j_{p_2} \end{array} \right\} \tag{63}$$

$$\int \mathrm{d}r_1\, r_1^2\, R^*_{p_1}(r_1)\, \omega^J_{p_1h_2}\, R_{h_2}(r_1) \sum_{iL} \delta_{t_i,t_{p_2}}\, (-1)^{j_i+\frac{1}{2}}\, \frac{1}{\widehat{L}^2}\, \gamma^L_{p_2 i}\, \gamma^L_{ih_1}\, \mathcal{J}_L^{[p_2 i];[ih_1]}\,,$$

$$D^{(2\mathrm{p}2\mathrm{h})}_{3.11}[p_1h_1p_2h_2] \;=\; 4\pi\, \delta_{t_{p_2},t_{h_1}}\, \delta_{j_{p_2},j_{h_1}}\, (-1)^{j_{p_1}+j_{h_2}+J+1}\, \widehat{J}_p\, \widehat{J}_h\, \xi(l_{p_2}+l_{h_1}) \left\{ \begin{array}{ccc} J_p & J_h & J \\ j_{h_2} & j_{p_1} & j_{p_2} \end{array} \right\} \int \mathrm{d}r_1\, r_1^2\, R^*_{p_1}(r_1)\, \omega^J_{p_1h_2}\, R_{h_2}(r_1)\, \mathcal{J}_0^{[p_2h_1];[\rho]}\,. \tag{64}$$

Also in this case the contribution of the electromagnetic charge and current operator to the two nucleon emission responses has to be calculated by inserting Eqs. (25)-(27) in the above equations. The explicit expressions we have obtained are given in Appendix B.

5 Specific applications

The model described above has been applied to evaluate electromagnetic responses and cross sections in the quasi-elastic region for the doubly magic nuclei ^{16}O and ^{40}Ca.

The two-body correlation function and the single particle basis are the two inputs necessary to build the many-body wavefunctions used in the calculation of the responses. In our calculations the set of single particle wave functions have been generated by a spherical Woods-Saxon potential of the form:

$$V(r) \;=\; V_0 F(r) \;+\; \left(\frac{\hbar c}{m_\pi}\right)^2 \frac{V_{LS}}{r}\, \frac{\mathrm{d}}{\mathrm{d}r} F(r)\; \mathbf{l}\cdot\boldsymbol{\sigma} \;+\; V_C(r)\,, \tag{65}$$

where m_π is the pion mass, $V_C(r)$ the Coulomb potential produced by a homogeneously charged sphere of radius R, and

$$F(r) \;=\; \frac{1}{1+e^{(r-R)/a}}\,. \tag{66}$$

The same parameterization of the potential has been used for both bound and continuum waves.

As we have already anticipated, the other input of our approach, the two-body correlation function, is a purely scalar function. Single particle waves and correlation functions are not independent quantities. In the theoretical framework of the CBF theory they are fixed by the minimization of the ground state energy functional. In our calculations we use wave functions and correlations taken from CBF-FHNC calculations of ^{16}O and ^{40}Ca ground states done with different hamiltonians.

A first set of many-body wavefunctions has obtained in Ref. [23] with the semi-realistic S3 interaction of Afnan and Tang. Specifically, we used the Woods-Saxon parameters of Tab. 5 of that reference together with the correlations labelled Euler in Tab. 6. We should recall that in that calculation the Woods-Saxon parameterizations was taken from the literature and the energy minimum was obtained by changing only the correlation function.

The second set of wave functions has been taken from Ref.[9] where a hamiltonian containing a V8' Argonne potential, which is a truncated version of the V18 interaction, together with the Urbana IX three-body interaction has been used. Our calculations have been done with the wavefunctions of Tab. V of that reference. Also in this case the Woods-Saxon parameters have been kept fixed and the energy minimum was found by changing only the correlation function. We should remark however that the energy minima found in these restricted calculations are only 7% larger than the those found by the full minimization. In our calculations we used only the scalar terms of the correlation functions of Ref. [9] which consider the channels of Eq. (9) up to $p = 6$.

Henceforth we shall label S3 and V8 all the quantities related to the wavefunctions of Ref.[23] and [9] respectively. We show in Fig. 3 the correlation functions $f(r)$ and we give in Tab. 1 the values of the parameters of the Woods-Saxon well. To complete the information on the input, we present in Tab. 2 and 3 the values of the single particle energies and we compare in Fig. 4 the MF and the correlated charge density distributions with the empirical densities of Ref. [24]. The charge densities have been obtained by folding the pointlike proton densities with the electromagnetic nucleon form factor of Ref. [25]. The same nucleon form factor has been used in the calculation of the responses.

Since the convection current contribution is already small at the MF level, as we show in Fig. 5, we did not consider the correlated terms produced by this current. In any case the convection current is included in the mean-field (MF) term.

5.1 One-nucleon emission

In Figs. 6, 7, 8, and 9 we present the electromagnetic 1p-1h responses calculated for the two nuclei considered for three different values of the the momentum transfer.

In these figures the full lines indicate the MF results. The dotted lines have been obtained by adding to the MF responses the contribution of two-point diagrams of Fig. 1, while the dashed lines show the results of the calculations when all the diagrams have been considered.

It is evident that the short-range correlations produce small effects on the inclusive responses. In the peak positions we found maximum relative variations with respect to the MF responses of 1.7% in the longitudinal and of 2.2% in the transverse responses. These values are within the range of the uncertainty produced by the different choices of nucleon form factors [26]. In spite of this we made a detailed investigation of the correlation effects because they can be relevant in the study of exclusive experiments.

In order to have a better view of the correlation effects we show in Figs. 10 and 11 the difference between the correlated and MF responses:

$$\Delta R_{L,T}(q,\omega) \;=\; R_{L,T}(q,\omega) - R^{\rm MF}_{L,T}(q,\omega)\,. \tag{67}$$

In these figures we have used the convention of indicating with the dotted lines the results obtained with the two-point diagrams only, and with the dashed line those obtained with all the diagrams.

The inclusion of the three-point diagrams reduces the effects produced by the two-point diagrams alone. This fact is most evident in the longitudinal responses and it is consistent with the findings of Refs. [27, 28] where ground state charge and momentum distributions have been studied. As discussed in sect. 3, the proper normalization of the many-body wave functions is obtained because in the limit for q $\rightarrow$ 0 the three-point diagrams cancel exactly the contribution of the two-point diagrams. This cancellation is present also for large values of the momentum transfer, but it is not exact any more. It is interesting to notice that the final correlated longitudinal responses are always smaller than the MF responses with the only exception of the S3 result in ^{40}Ca at 300 MeV/c.

The behavior of the correlations on the transverse responses is rather different: the correlated responses are always larger than the MF ones. The reason of this behavior has to be ascribed to the diagram (2.3) of Fig. 1 which does not contributes in the transverse response as indicated in Appendix A. In this diagram the exchanged virtual photon strikes a nucleon which remains bound but through the correlation it excites a p-h pair producing the nucleon emission. Since in our calculations the correlation is a scalar function, only longitudinally polarized virtual photons can induce this type of excitation.

To study the effect of this diagram we set it artificially to zero also in the longitudinal channel. The comparison with the correctly calculated longitudinal response is shown in Fig. 12 for the ^{16}O response at $q = 400$ MeV/c calculated with the S3 wavefunctions. In the upper panel we show the responses, and in the lower one the ΔR_l of Eq. (67). The (2.3) diagram lowers the response and produces the discussed difference between longitudinal and transverse responses. The curves without the contribution of the (2.3) diagram in the lower panel are very similar to the analogous ones of Fig. 10 for the transverse responses.

Another interesting feature observed in Figs. 10 and 11 is the different behavior shown by the S3 and V8 correlations. The two-point contributions of the S3 correlation are always positive, and the S3 total contributions are always larger than those of the V8.

The different features characterizing the two correlation functions are shown in Fig. 3. A first difference concerns the behavior at $r = 0$ where the S3 correlations assume larger values than the V8 ones. The second difference is related to the behavior at r values around 1-1.5 fm, where the S3 correlation functions show a sizable overshooting with respect to the asymptotic value of 1. In order to study the effects of these two features on the response functions, we performed calculations using correlation functions of the form:

$$f(r) = 1 - A\exp[-Br^2] + C\exp[-D(r-r_0)^2]\,. \tag{68}$$

This expression allowed us to disentangle and magnify the characteristics of the correlation function under investigation by changing the values of the parameters. The values used in our calculations are given in Table 4. The correlations g1, g2 and g3, shown in the upper panel of Fig. 13, are composed only by a single gaussian and have been constructed to change only the behavior at $r = 0$. The other correlations, shown in the lower panel of Fig. 13, have the same behavior at $r = 0$ but have different overshooting properties at intermediate distances. With these correlations we calculated the ^{16}O responses at q=400 MeV/c using the S3 set of single particle wave functions. The results of these calculations are summarized in Fig. 14 where the $\Delta R_{L,T}$ defined in Eq. (67) are shown as functions of the excitation energy.

The two upper panels of the figure show the effect produced by changing the correlation depth at $r = 0$. The global effect is a reduction of the MF responses, more evident in the longitudinal one. The reduction is larger for deeper correlations. The other two panels of the figure show the effects of the overshooting. There is a slight depletion of the longitudinal MF responses and an enhancement of the transverse ones. The effects are magnified by shifting the overshooting at larger distances. This figure clearly shows the role of the three-point diagrams which always reduce the effects of the correlations.

To compare of our results with experimental data it is necessary to consider the effects of the rescattering of the emitted nucleon with the rest nucleus [29]. We describe these Final State Interactions (FSI) effects with the method developed in Refs. [20, 21]. The method shows that, under certain approximations, it is possible to consider the FSI by folding the bare responses with a smoothing function:

$$R^{\rm FSI}(q,\omega) = \frac{M^*}{M}\int_0^\infty dE\, R(q,E)\left[\rho\left(E,\frac{M^*}{M}\omega\right) + \rho\left(E,-\frac{M^*}{M}\omega\right)\right]\,, \tag{69}$$

where we have indicated with M and M^* the free and effective nucleon masses respectively, and where the function $\rho(E,\omega)$ describing the effects of FSI is:

$$\rho(E,\omega) = \frac{1}{2\pi}\frac{\Gamma(\omega)}{[E-\omega-\Delta(\omega)]^2 + [\Gamma(\omega)/2]^2}\,. \tag{70}$$

The $\Delta(\omega)$ and $\Gamma(\omega)$ functions of the above equation are connected by a dispersion relation:

$$\Delta(\omega) = \frac{1}{2\pi}\mathcal{P}\int_{-\infty}^{+\infty} d\omega'\,\frac{\Gamma(\omega')}{\omega'-\omega}\,, \tag{71}$$

where $\mathcal{P}$ indicates the principal value of the integral. The function $\Gamma(\omega)$ is related to the imaginary part of the single particle self-energy. We have obtained $\Gamma(\omega)$ as average of the single particle energy width $\gamma(\omega)$:

$$\Gamma(\omega) = \frac{1}{\omega}\int_0^\infty d\epsilon\,[\gamma(\epsilon+\omega) + \gamma(\epsilon-\omega)]\ . \tag{72}$$

The single particle energy has not been calculated with a microscopic model, but, following Ref.[30], has been parametrized as follows to reproduce empirical values:

$$\gamma(\epsilon) = a\cdot\frac{\epsilon^2}{\epsilon^2+b^2}h(\epsilon)\,, \tag{73}$$

with $a = 11.5$ and $b = 18$.

The effective nucleon mass takes into account non-locality effects of the mean-field which cannot be neglected. We determined the value of the effective nucleon mass by using the expressions proposed in the polarization potential model of Ref. [31]:

$$\frac{M^*}{M} = \frac{1}{1+2M\Delta U/(q^2+q_0^2)}\,, \tag{74}$$

with

$$q_0^2 = \frac{2M\Delta U}{M/M_0^* - 1}\,, \tag{75}$$

ΔU=50 MeV and $M_0^* = 0.8M$.

In Fig. 15 we compare our ^{40}Ca longitudinal and transverse responses with the data of Refs. [32] and [33]. Dashed (full) lines show the results of the S3 (V8) calculations. Both results are in a reasonable agreement with the data. The differences between the two calculations are mainly produced by the differences in the mean-field basis rather than in the correlation functions.

For the nucleus ^{16}O, Rosenbluth separated data for longitudinal and transverse responses are not available. In Fig. 16 we compare our results with the cross section data taken at Frascati [34]. These data have been measured for fixed values of the incident electron energy and of the scattering angle and, therefore, the value of the momentum transfer changes at every excitation energy. Since the data have been taken at the scattering angle of 32^o, the average momentum value for the cross section at ϵ=700 MeV is about 400 MeV/c and that at ϵ=1200 MeV is about 650 MeV/c.

The folding method used to consider FSI is thought for fixed values of the momentum transfer. Every cross section point has been calculated by fixing the value of q, calculating the response on a wide energy range (up to 400 MeV), folding the response with Ed. (69), and extracting from this output the single result at the appropriate excitation energy value. The responses calculated in this way have been inserted in Eq. (16).

Also in Fig. 16 the full (dashed) lines show the results obtained with the V8 (S3) input. The agreement with the data is satisfactory, especially for the cross sections measured at higher energies. The differences between the S3 and V8 results are even smaller than in the case of ^{40}Ca and the data cannot discriminate between them.

5.2 Two-nucleon emission

The study of the two-nucleon emission responses is limited by the heavy computational load. For this reason we have restricted our investigation to the ^{16}O nucleus only.

For these calculations we used the same configuration space considered in the one-nucleon emission calculations. This includes all the protons and neutrons waves with $l \leq 14$. Within this configuration space all the excitation multipoles compatible with angular momentum coupling of the 2p-2h excitation pairs have been considered (see Eq. (55)).

We found that the contribution of the various partial waves becomes smaller the higher is the angular momentum value. Specifically, we have seen that for $q \sim 600$ MeV/c the contribution of partial waves with $l > 4$ is about the 2% of the total value at an excitation energy of 100 MeV and becomes about the 40% at the excitation energy of 300 MeV. These percentiles remain roughly constant in the momentum transfer range between 400 and 600 MeV/c. In order to reduce the computational time we performed a complete calculation for the partial waves with $l \leq 4$ while we made a statistical evaluation of the contribution of the higher partial waves. This statistical evaluation consist in calculating a randomly chosen 10% of the 2p-2h matrix elements, and in rescaling the obtained results proportionally to the total number of the matrix elements to be calculated. This simplification reduced by 2/3 the computational time. We have tested the reliability of this simplifying technique by calculating all the 2p-2h matrix elements at the excitation energies of 100, 200 and 300 MeV. In all the cases investigated we found differences with respect to the simplified calculations smaller than 1%.

The calculations of the two-nucleon emission responses have been done for both correlation functions at the excitation energies of 100, 140, 200, 240 and 300 MeV for the kinematical conditions used to evaluate the inclusive cross sections of Fig. 16 at ϵ = 700 and 1080 MeV. The values of the responses obtained in these calculations are shown in Fig. 17 by the squares (S3) and by the circles (V8).

A direct comparison with the results of Ref. [35] is not straightforward since the calculations of that reference have been done on the ^{12}C nucleus, and obviously, with different inputs. Considering these differences we can say that the order of magnitude of two calculations is the same. In the two calculations it is however remarkably different the contribution of the three-point diagrams. We found a maximum contribution to R_L of about the 8% and even smaller, the 1%, for the transverse response. In the longitudinal response the interference between two- and three-point diagrams is always destructive, therefore the final response is always smaller than that of the two-point diagrams alone. The contradiction with the findings of Ref. [35], where the three-point diagrams were giving an important contribution to the response, was produced by a computer error we found in our previous calculations.

The results of Fig. 17 show a large sensitivity to the choice of the correlation. This is not surprising since in these calculations the two-nucleon emission is produced only by means of the short range correlation. We have also verified the sensitivity to the choice of the mean-field by calculating responses with V8 correlation and S3 mean-field for ϵ=1080 MeV. The results obtained in this way are shown in Fig. 17 by the triangles. The changes of the mean-field wave functions affect considerably the final result.

The two-nucleon emission responses have been used to calculate the inclusive cross section. The total responses have been obtained by adding one- and two-nucleon emission responses. To make this sum we have interpolated the results of Fig. 17 in order to obtain the values of the 2p-2h responses at the desired excitation energies. We have used linear and quadratic interpolations and their results are shown in Fig. 17 by the dashed and full lines respectively. These interpolations as well as more sophisticated interpolation techniques we have also used produce results which are the same within the accuracy of the calculations. For the evaluation of the cross section we used the results of the quadratic interpolation.

The comparison of the results of Fig. 17 with those of Figs. 6 and 7 shows that the 2p-2h responses at the peak energy are two orders of magnitude smaller than the 1p-1h ones. The contribution of two-nucleon emission becomes relevant only at higher energies, in the dip region. As example, we show in Fig. 18 the contribution of the various V8 responses in the dip region for the two kinematical cases we have considered. The dashed lines represent the tail of the 1p-1h responses while the dashed-dotted lines the contribution of the 2p-2h responses. The full lines are the sum of the two. It is interesting to notice the different behavior of the responses for the cases at 700 and 1080 MeV. In the first case, for excitation energies above 220 MeV the 2p-2h responses become larger than the 1p-1h ones. For ϵ=1080 MeV the 1p-1h responses remain always larger than the 2p-2h ones. This different behavior is produced by the larger value of the momentum transverse in this last case which shifts the 1p-1h responses to higher energies. For this reason the tail of this response has not yet died out as in the 700 MeV case.

The calculation of the cross section requires the inclusion of the FSI effects. We have treated them with the folding model previously described. There is an ambiguities in our procedure of including the FSI interaction. We could apply the folding procedure to the total responses or separately to the 1p-1h and 2p-2h responses and then sum the two folded responses. The two procedures gave results differing only few percent. We show in Fig. 19 the tail of the calculated cross sections. The dashed lines present the pure 1p-1h results while the full lines have been obtained by including also the 2p-2h contribution. The effects of the 2p-2h responses which appeared in Fig.18 are washed out by the inclusion of the FSI, whose effects are much larger than those produced by the short range correlations. The inclusion of two-nucleon emission responses does not modify the comparison with the experimental data shown in Fig. 16.

6 Conclusions

In this paper we have presented a model to evaluate the effects of the short-range correlations in the excitation of the one-body nuclear responses. Our model takes into account both two- and tree-body diagrams where the short-range correlations appear at the first order. We have shown that both kinds of diagrams are necessary to have properly normalized wave functions.

As input of our calculations we have used scalar (Jastrow) correlation functions and single particle wave functions fixed in Refs. [23] and [9] by a minimization of the nuclear ground state energy.

The model has been applied to evaluate the inclusive electromagnetic longitudinal and transverse responses in the quasi-elastic region for the ^{16}O and ^{40}Ca nuclei. We have considered both one- and two-nucleon emission channels. The longitudinal response has been calculated using the charge operator. In the transverse response we have considered the magnetization current and we have included the convection current only in the uncorrelated diagram.

Our results show that the effect of the correlations on the one-particle emission responses is small, certainly within the range of uncertainty related to the different choices of the electromagnetic nucleon form factors. In spite of this, we made a detailed investigation of short-range correlations effects in our model because they can be relevant in exclusive processes.

The three-point diagrams, usually neglected in the literature, interfere destructively with the two-point diagrams. For this reason any effect produced by the two-point diagrams is always reduced when the three-point ones are included. In certain situations this reduction is of the order of 80%.

Our calculations show that the correlations act differently on longitudinal and transverse responses. Specifically, we found that the longitudinal responses are lowered while the transverse ones are enhanced. This happens because some of the three-point diagrams do not contribute in the longitudinal response.

We have calculated the inclusive cross sections in ^{16}O to compare our results with the data of Ref. [34]. In ^{40}Ca the comparison has been done directly with the empirical responses of Ref. [33]. In both cases the agreement with the data is quite satisfactory independently from the inclusion of the short-range correlations.

The two-nucleon emission responses have been calculated only for the ^{16}O nucleus. Because of the heavy computational load we have simplified the calculation by evaluating the most important matrix elements and providing a statistical estimation of the others.

Like in the one-nucleon emission case, also in the two-nucleon emission responses, the two- and three-point diagrams produce effects with opposite sign. However, in this case we found that the contribution of the three-point diagrams is at most of the order of few percents of that of the two-point diagrams.

In the quasi-elastic region, our calculations show that the 2p-2h responses are two order of magnitude smaller than the 1p-1h ones.

Summarizing our results, we should say that a proper normalization of the many body wave function in a first order expansion model for the correlations, requires the inclusion of the three-body terms. The contribution of these terms always reduces the effect produced by the two-point diagrams. This effect is not negligible in the one-nucleon emission responses, but it becomes rather small in the two-nucleon emission.

The use of different correlations, together with different set of single particle wave functions, has clearly shown the sensitivity of the results to both parts of the input of the calculations. This is true not only in the 1p-1h responses, where the result was expected since they are dominated by the uncorrelated terms, but also in the 2p-2h responses, where the uncorrelated term is not present. Physically meaningful results can be obtained only if single particle wave functions and short range correlations are linked through the nuclear hamiltonian.

In our calculations the presence of short-range correlations does not produce remarkable effects. There are other effects beyond the pure mean-field model, such as final state interactions and meson exchange currents [37], which are more important. We should however point out that we have used only scalar correlation functions. There are indications that state dependent correlations together with MEC [36] could produce sizable effects.

The next step of our work will be to apply the model to the description of exclusive electron scattering experiments, (e,e'N) and (e,e'2N), where one expects that the effects of the short-range correlations could be disentangled.

7 Acknowledgments

We thank M. Anghinolfi and C.F. Williamson for providing us with the experimental data and J. E. Amaro, F. Arias de Saavedra, A. Fabrocini and S.M. Rashad for useful discussions. G.C. thanks the University of Granada for the hospitality during his visit. This work has been partially supported by the CYCIT-INFN agreement and by the DGES (PB98-1367) and the Junta de Andalucía (FQM225).

Appendix A. One-particle emission matrix elements

In this appendix we give the expressions of the matrix elements involved in the one-nucleon emission part of the longitudinal and transverse responses. As discusses in Sect. 4, only the charge operator contributes to the longitudinal response, while both the electric and magnetic parts of the magnetization current, Eqs. (26,27), contribute to transverse response. The convection current is considered in the one-point diagram only.

We begin with the Coulomb (charge) matrix elements for which we have:

$$M_1^{(1p1h)} = G_E^p(q^2)\,\delta_{t_p,t_h}\,\gamma_{ph}^J\,\mathcal{I}_J^{[ph]}(q)\,, \tag{76}$$

$$M_{2.1}^{(1p1h)} = G_E^p(q^2)\,\delta_{t_p,t_h}\,4\pi\,\gamma_{ph}^J\,\mathcal{I}_{J0}^{[ph];[\rho]}(q)\,, \tag{77}$$

$$M_{2.2}^{(1p1h)} = G_E^p(q^2)\,\delta_{t_p,t_h}\,\gamma_{ph}^J \sum_{iL} \delta_{t_i,t_p}\,\xi(l_i+l_h+L)\,\widehat{j}_i^2 \left(\begin{array}{ccc} j_i & j_h & L \\ \frac{1}{2} & -\frac{1}{2} & 0 \end{array}\right)^2 \mathcal{I}_{JL}^{[pi];[ih]}(q)\,, \tag{78}$$

$$M_{2.3}^{(1p1h)} = \delta_{t_p,t_h}\,4\pi\,\gamma_{ph}^J\,\frac{1}{\widehat{J}^2}\,\mathcal{I}_{JJ}^{[\rho_{\rm ch}];[ph]}(q)\,, \tag{79}$$

$$M_{2.4}^{(1p1h)} = G_E^p(q^2)\,\delta_{t_p,t_h}\,\gamma_{ph}^J \sum_{iL} \delta_{t_i,t_p}\,\xi(l_p+l_i+L)\,\widehat{j}_i^2 \left(\begin{array}{ccc} j_p & j_i & L \\ \frac{1}{2} & -\frac{1}{2} & 0 \end{array}\right)^2 \mathcal{I}_{JL}^{[ih];[pi]}(q)\,, \tag{80}$$

$$M_{3.1}^{(1p1h)} = G_E^p(q^2)\,\delta_{t_p,t_h}\,\gamma_{ph}^J \sum_{ikL} \delta_{t_i,t_p}\,\delta_{t_k,t_p}\,\delta_{j_i,j_p}\,\xi(l_p+l_k+L)\,\xi(l_p+l_i)\,\widehat{j}_k^2 \left(\begin{array}{ccc} j_p & j_k & L \\ \frac{1}{2} & -\frac{1}{2} & 0 \end{array}\right)^2 \mathcal{I}_J^{[ih]}(q)\ \mathcal{J}_L^{[pk];[ki]}\,, \tag{81}$$

$$M_{3.2}^{(1p1h)} = G_E^p(q^2)\,\delta_{t_p,t_h}\,4\pi\,\gamma_{ph}^J \sum_{i} \delta_{t_i,t_p}\,\delta_{j_i,j_p}\,\xi(l_p+l_i)\ \mathcal{I}_J^{[ih]}(q)\ \mathcal{J}_0^{[pi];[\rho]}\,, \tag{82}$$

$$M_{3.3}^{(1p1h)} = G_E^p(q^2)\,\delta_{t_p,t_h}\,\gamma_{ph}^J \sum_{ikL} \delta_{t_i,t_p}\,\delta_{t_k,t_p}\,\delta_{j_i,j_h}\,\xi(l_k+l_h+L)\,\xi(l_i+l_h)\,\widehat{j}_k^2 \left(\begin{array}{ccc} j_k & j_h & L \\ \frac{1}{2} & -\frac{1}{2} & 0 \end{array}\right)^2 \mathcal{I}_J^{[pi]}(q)\ \mathcal{J}_L^{[kh];[ik]}\,, \tag{83}$$

$$M_{3.4}^{(1p1h)} = G_E^p(q^2)\,\delta_{t_p,t_h}\,4\pi\,\gamma_{ph}^J \sum_{i} \delta_{t_i,t_p}\,\delta_{j_i,j_h}\,\xi(l_i+l_h)\ \mathcal{I}_J^{[pi]}(q)\ \mathcal{J}_0^{[ih];[\rho]}\,, \tag{84}$$

$$M_{3.5}^{(1p1h)} = G_E^p(q^2)\,\delta_{t_p,t_h}\,4\pi \sum_{ikL} \delta_{t_i,t_p}\,\delta_{t_k,t_p}\,(-1)^{j_i+j_k+J+L}\,\frac{1}{\widehat{L}^2}\,\gamma_{ik}^J\,\gamma_{pi}^L\,\gamma_{kh}^L \tag{85}$$

$$\left\{ \begin{array}{ccc} j_p & j_h & J \\ j_k & j_i & L \end{array} \right\} \mathcal{I}_J^{[ik]}(q)\, \mathcal{J}_L^{[pi];[kh]} \,,$$

$$M_{3.6}^{(\mathrm{1p1h})} \;=\; \delta_{t_p,t_h}\, 4\pi\, \frac{1}{\widehat{J}^4}\, \gamma_{ph}^J \sum_{ik} \delta_{t_i,t_k}\, G_E^i(q^2)\, (\gamma_{ik}^J)^2 \mathcal{I}_J^{[ik]}(q)\, \mathcal{J}_J^{[ph];[ki]} \,. \tag{86}$$

In the previous equations we have indicated with $G_E^\alpha(q^2)$ the electric form factor of the nucleon in the single particle state α, and we have defined the integrals

$$\mathcal{I}_J^{[\alpha\beta]}(q) \;=\; \int \mathrm{d}r\, r^2\, j_J(qr)\, R_\alpha^*(r)\, R_\beta(r)\,, \tag{87}$$

$$\mathcal{I}_{JL}^{[\alpha\beta];[\gamma\delta]}(q) \;=\; \int \mathrm{d}r_1\, r_1^2\, j_J(qr)\, R_\alpha^*(r_1)\, R_\beta(r_1)\, \mathcal{H}_L^{[\gamma\delta]}(r_1)\,, \tag{88}$$

$$\mathcal{I}_{J0}^{[\alpha\beta];[\rho]}(q) \;=\; \int \mathrm{d}r_1\, r_1^2\, j_J(qr)\, R_\alpha^*(r_1)\, R_\beta(r_1)\, \mathcal{H}_0^{[\rho]}(r_1)\,, \tag{89}$$

$$\mathcal{I}_{JJ}^{[\rho_{\mathrm{ch}}];[\gamma\delta]}(q) \;=\; \int \mathrm{d}r_1\, r_1^2\, j_J(qr)\, \rho_{\mathrm{ch}}(r_1)\, \mathcal{H}_J^{[\gamma\delta]}(r_1)\,, \tag{90}$$

where $j_J(x)$ is a spherical Bessel function, $\mathcal{H}_L^{[\gamma\delta]}(r)$ is given by Eq. (44), $\mathcal{H}_0^{[\rho]}(r)$ is given by Eq. (45), and

$$\rho_{\mathrm{ch}}(r) \;=\; G_E^{\mathrm{prot}}(q^2)\, \rho_{\mathrm{prot}}(r) \;+\; G_E^{\mathrm{neut}}(q^2)\, \rho_{\mathrm{neut}}(r)\,, \tag{91}$$

with $\rho_{\mathrm{prot}}(r)$ and $\rho_{\mathrm{neut}}(r)$ the proton and neutron densities, respectively. Finally, the integrals $\mathcal{J}$ are defined in Eqs. (53,54).

The matrix elements of the transverse electric part of the magnetization current are given by:

$$T_{1;m}^{\mathrm{E(1p1h)}}1 \;=\; -q\, \frac{G_M^p(q^2)}{2M_p}\, \delta_{t_p,t_h}\, \gamma_{ph}^J\, \frac{\chi_p - \chi_h}{\sqrt{J(J+1)}}\, \mathcal{I}_J^{[ph]}(q)\,, \tag{92}$$

$$T_{2.1;m}^{\mathrm{E(1p1h)}} \;=\; -q\, \frac{G_M^p(q^2)}{2M_p}\, \delta_{t_p,t_h}\, 4\pi\, \gamma_{ph}^J\, \frac{\chi_p - \chi_h}{\sqrt{J(J+1)}}\, \mathcal{I}_{J0}^{[ph];[\rho]}(q)\,, \tag{93}$$

$$\begin{aligned} T_{2.2;m}^{\mathrm{E(1p1h)}} \;=\;& q\, \frac{G_M^p(q^2)}{2M_p}\, \delta_{t_p,t_h} \sqrt{\frac{3}{\pi}}\, (-1)^{l_p+j_p+J+\frac{1}{2}}\, \widehat{l}_p\, \widehat{j}_p\, \widehat{j}_h\, \widehat{J} \sum_{iL} \delta_{t_i,t_p}\, \xi(l_i+l_h+L)\, \widehat{l}_i\, \widehat{j}_i^2 \\ & \left(\begin{array}{ccc} j_i & j_h & L \\ \frac{1}{2} & -\frac{1}{2} & 0 \end{array} \right) \mathcal{I}_{JL}^{[pi];[ih]}(q) \sum_\lambda \xi(L+J+\lambda)\, \widehat{\lambda}^2 \left(\begin{array}{ccc} l_p & l_i & \lambda \\ 0 & 0 & 0 \end{array} \right) \\ & \sum_K \widehat{K}^2 \left\{ \begin{array}{ccc} L & K & J \\ j_p & j_h & j_i \end{array} \right\} \left(\begin{array}{ccc} 1 & K & \lambda \\ 1 & -1 & 0 \end{array} \right) \left(\begin{array}{ccc} K & J & L \\ 1 & -1 & 0 \end{array} \right) \left\{ \begin{array}{ccc} l_p & \frac{1}{2} & j_p \\ l_i & \frac{1}{2} & j_i \\ \lambda & 1 & K \end{array} \right\}, \end{aligned} \tag{94}$$

$$T_{2.3;m}^{\mathrm{E(1p1h)}} \;=\; 0\,, \tag{95}$$

$$\begin{aligned} T_{2.4;m}^{\mathrm{E(1p1h)}} \;=\;& q\, \frac{G_M^p(q^2)}{2M_p}\, \delta_{t_p,t_h} \sqrt{\frac{3}{\pi}}\, (-1)^{l_p+j_p+j_h}\, \widehat{l}_h\, \widehat{j}_p\, \widehat{j}_h\, \widehat{J} \sum_{iL} \delta_{t_i,t_p}\, (-1)^{j_i-\frac{1}{2}}\, \xi(l_p+l_i+L) \\ & \widehat{l}_i\, \widehat{j}_i^2 \left(\begin{array}{ccc} j_p & j_i & L \\ \frac{1}{2} & -\frac{1}{2} & 0 \end{array} \right) \mathcal{I}_{JL}^{[ih];[pi]}(q) \sum_\lambda \xi(L+J+\lambda)\, \widehat{\lambda}^2 \left(\begin{array}{ccc} l_i & l_h & \lambda \\ 0 & 0 & 0 \end{array} \right) \end{aligned} \tag{96}$$

$$\sum_K (-1)^K \,\widehat{K}^2 \left\{ \begin{array}{ccc} L & K & J \\ j_h & j_p & j_i \end{array} \right\} \left(\begin{array}{ccc} 1 & K & \lambda \\ 1 & -1 & 0 \end{array} \right) \left(\begin{array}{ccc} K & J & L \\ 1 & -1 & 0 \end{array} \right) \left\{ \begin{array}{ccc} l_i & \frac{1}{2} & j_i \\ l_h & \frac{1}{2} & j_h \\ \lambda & 1 & K \end{array} \right\},$$

$$T^{\mathrm{E(1p1h)}}_{3.1;m} = -q\,\frac{G^p_M(q^2)}{2M_p}\,\delta_{t_p,t_h}\,\gamma^J_{ph}\,\frac{\chi_p-\chi_h}{\sqrt{J(J+1)}}\sum_{ikL}\delta_{t_i,t_p}\,\delta_{t_k,t_p}\,\delta_{j_i,j_p} \tag{97}$$
$$\xi(l_p+l_k+L)\,\xi(l_p+l_i)\,\widehat{j}_k^2 \left(\begin{array}{ccc} j_p & j_k & L \\ \frac{1}{2} & -\frac{1}{2} & 0 \end{array} \right)^2 \mathcal{I}^{[ih]}_J(q)\,\mathcal{J}^{[pk];[ki]}_L\,,$$

$$T^{\mathrm{E(1p1h)}}_{3.2;m} = -q\,\frac{G^p_M(q^2)}{2M_p}\,\delta_{t_p,t_h}\,4\pi\,\gamma^J_{ph}\,\frac{\chi_p-\chi_h}{\sqrt{J(J+1)}}\sum_{i}\delta_{t_i,t_p}\,\delta_{j_i,j_p}\,\xi(l_p+l_i) \tag{98}$$
$$\mathcal{I}^{[ih]}_J(q)\,\mathcal{J}^{[pi];[\rho]}_0\,,$$

$$T^{\mathrm{E(1p1h)}}_{3.3;m} = -q\,\frac{G^p_M(q^2)}{2M_p}\,\delta_{t_p,t_h}\,\gamma^J_{ph}\,\frac{\chi_p-\chi_h}{\sqrt{J(J+1)}}\sum_{ikL}\delta_{t_i,t_p}\,\delta_{t_k,t_p}\,\delta_{j_i,j_h} \tag{99}$$
$$\xi(l_k+l_h+L)\,\xi(l_i+l_h)\,\widehat{j}_k^2 \left(\begin{array}{ccc} j_k & j_h & L \\ \frac{1}{2} & -\frac{1}{2} & 0 \end{array} \right)^2 \mathcal{I}^{[pi]}_J(q)\,\mathcal{J}^{[kh];[ik]}_L\,,$$

$$T^{\mathrm{E(1p1h)}}_{3.4;m} = -q\,\frac{G^p_M(q^2)}{2M_p}\,\delta_{t_p,t_h}\,4\pi\,\gamma^J_{ph}\,\frac{\chi_p-\chi_h}{\sqrt{J(J+1)}}\sum_{i}\delta_{t_i,t_p}\,\delta_{j_i,j_h}\,\xi(l_i+l_h) \tag{100}$$
$$\mathcal{I}^{[pi]}_J(q)\,\mathcal{J}^{[ih];[\rho]}_0\,,$$

$$T^{\mathrm{E(1p1h)}}_{3.5;m} = -q\,\frac{G^p_M(q^2)}{2M_p}\,\delta_{t_p,t_h}\,4\pi\,\frac{1}{\sqrt{J(J+1)}}\sum_{ikL}\delta_{t_i,t_p}\,\delta_{t_k,t_p}\,(-1)^{j_i+j_k+J+L}\,\frac{\chi_i-\chi_k}{\widehat{L}^2} \tag{101}$$
$$\gamma^J_{ik}\,\gamma^L_{pi}\,\gamma^L_{kh} \left\{ \begin{array}{ccc} j_p & j_h & J \\ j_k & j_i & L \end{array} \right\} \mathcal{I}^{[ik]}_J(q)\,\mathcal{J}^{[pi];[kh]}_L\,,$$

$$T^{\mathrm{E(1p1h)}}_{3.6;m} = -\delta_{t_p,t_h}\,4\pi\,\frac{1}{\widehat{J}^4\sqrt{J(J+1)}}\,\gamma^J_{ph}\sum_{ik}\delta_{t_i,t_k}\,q\,\frac{G^i_M(q^2)}{2M_i}\,(\chi_i-\chi_k)\,(\gamma^J_{ik})^2 \tag{102}$$
$$\mathcal{I}^{[ik]}_J(q)\,\mathcal{J}^{[ph];[ki]}_J\,.$$

In these equations we have indicated with $G^\alpha_M(q^2)$ the magnetic form factor of the nucleon in the single particle state α, and with M_α. The symbol χ_α has been defined as:

$$\chi_\alpha = (l_\alpha - j_\alpha)\,(2j_\alpha+1)\,. \tag{103}$$

For the transverse magnetic part of the magnetization current the corresponding matrix elements are:

$$T^{\mathrm{M(1p1h)}}_{1;m} = -iq\,\frac{G^p_M(q^2)}{2M_p}\,\delta_{t_p,t_h}\,\eta^J_{ph}\,\frac{1}{\widehat{J}^2} \tag{104}$$
$$\sum_{s=\pm1} s\,\sqrt{\frac{J+\delta_{s,-1}}{J+\delta_{s,1}}}\,(\chi_p+\chi_h+sJ+\delta_{s,1})\,\mathcal{I}^{[ph]}_{J'}(q)\,,$$

$$T^{\mathrm{M(1p1h)}}_{2.1;m} = -iq\,\frac{G^p_M(q^2)}{2M_p}\,\delta_{t_p,t_h}\,4\pi\,\eta^J_{ph}\,\frac{1}{\widehat{J}^2} \tag{105}$$

$$\sum_{s=\pm1} s\,\sqrt{\frac{J+\delta_{s,-1}}{J+\delta_{s,1}}}\,(\chi_p+\chi_h+sJ+\delta_{s,1})\,\mathcal{I}^{[ph];[\rho]}_{J'0}(q)\,,$$

$$\begin{aligned}
T^{\mathrm{M(1p1h)}}_{2.2;m} &= -iq\,\frac{G^p_M(q^2)}{2M_p}\,\delta_{t_p,t_h}\sqrt{\frac{3}{2\pi}}\,(-1)^{j_h+j_p}\,\widehat{l}_p\,\widehat{j}_p\,\widehat{j}_h \\
&\sum_{iL}\delta_{t_i,t_p}\,(-1)^{j_i+l_i+\frac{1}{2}}\,\xi(l_i+l_h+L)\,\widehat{l}_i\,\widehat{j}_i^2\begin{pmatrix} j_i & L & j_h \\ \frac{1}{2} & 0 & -\frac{1}{2}\end{pmatrix} \\
&\sum_{s=\pm1} s\,\sqrt{J+\delta_{s,-1}}\,\widehat{J}'\,\mathcal{I}^{[pi];[ih]}_{J'L}(q)\sum_{\lambda}\widehat{\lambda}^2\begin{pmatrix} l_p & l_i & \lambda \\ 0 & 0 & 0\end{pmatrix}\begin{pmatrix} L & J' & \lambda \\ 0 & 0 & 0\end{pmatrix} \\
&\sum_{K}(-1)^K\,\widehat{K}^2\begin{Bmatrix} L & K & J \\ j_p & j_h & j_i\end{Bmatrix}\begin{Bmatrix} L & J' & \lambda \\ 1 & K & J\end{Bmatrix}\begin{Bmatrix} l_p & \frac{1}{2} & j_p \\ l_i & \frac{1}{2} & j_i \\ \lambda & 1 & K\end{Bmatrix}\,,
\end{aligned}\tag{106}$$

$$T^{\mathrm{M(1p1h)}}_{2.3;m} = 0\,, \tag{107}$$

$$\begin{aligned}
T^{\mathrm{M(1p1h)}}_{2.4;m} &= -iq\,\frac{G^p_M(q^2)}{2M_p}\,\delta_{t_p,t_h}\sqrt{\frac{3}{2\pi}}\,(-1)^{j_h+\frac{1}{2}}\,\widehat{l}_h\,\widehat{j}_p\,\widehat{j}_h \\
&\sum_{iL}\delta_{t_i,t_p}\,(-1)^{l_i}\,\xi(l_p+l_i+L)\,\widehat{l}_i\,\widehat{j}_i^2\begin{pmatrix} j_p & L & j_i \\ \frac{1}{2} & 0 & -\frac{1}{2}\end{pmatrix} \\
&\sum_{s=\pm1} s\,\sqrt{J+\delta_{s,-1}}\,\widehat{J}'\,\mathcal{I}^{[ih];[pi]}_{J'L}(q)\sum_{\lambda}\widehat{\lambda}^2\begin{pmatrix} l_i & l_h & \lambda \\ 0 & 0 & 0\end{pmatrix}\begin{pmatrix} L & J' & \lambda \\ 0 & 0 & 0\end{pmatrix} \\
&\sum_{K}\widehat{K}^2\begin{Bmatrix} L & K & J \\ j_h & j_p & j_i\end{Bmatrix}\begin{Bmatrix} L & J' & \lambda \\ 1 & K & J\end{Bmatrix}\begin{Bmatrix} l_i & \frac{1}{2} & j_i \\ l_h & \frac{1}{2} & j_h \\ \lambda & 1 & K\end{Bmatrix}\,,
\end{aligned}\tag{108}$$

$$\begin{aligned}
T^{\mathrm{M(1p1h)}}_{3.1;m} &= -iq\,\frac{G^p_M(q^2)}{2M_p}\,\delta_{t_p,t_h}\,\eta^J_{ph}\,\frac{1}{\widehat{J}^2}\sum_{ikL}\delta_{t_i,t_p}\,\delta_{t_k,t_p}\,\delta_{j_i,j_p} \\
&\xi(l_p+l_k+L)\,\xi(l_p+l_i)\,\widehat{j}_k^2\begin{pmatrix} j_p & j_k & L \\ \frac{1}{2} & -\frac{1}{2} & 0\end{pmatrix}^2\mathcal{J}^{[pk];[ki]}_L \\
&\sum_{s=\pm1} s\,\sqrt{\frac{J+\delta_{s,-1}}{J+\delta_{s,1}}}\,(\chi_p+\chi_h+sJ+\delta_{s,1})\,\mathcal{I}^{[ih]}_{J'}(q)\,,
\end{aligned}\tag{109}$$

$$\begin{aligned}
T^{\mathrm{M(1p1h)}}_{3.2;m} &= -iq\,\frac{G^p_M(q^2)}{2M_p}\,\delta_{t_p,t_h}\,4\pi\,\eta^J_{ph}\,\frac{1}{\widehat{J}^2}\sum_{i}\delta_{t_i,t_p}\,\delta_{j_i,j_p}\,\xi(l_p+l_i)\,\mathcal{J}^{[pi];[\rho]}_0 \\
&\sum_{s=\pm1} s\,\sqrt{\frac{J+\delta_{s,-1}}{J+\delta_{s,1}}}\,(\chi_p+\chi_h+sJ+\delta_{s,1})\,\mathcal{I}^{[ih]}_{J'}(q)\,,
\end{aligned}\tag{110}$$

$$T^{\mathrm{M(1p1h)}}_{3.3;m} = -iq\,\frac{G^p_M(q^2)}{2M_p}\,\delta_{t_p,t_h}\,\eta^J_{ph}\,\frac{1}{\widehat{J}^2}\sum_{ikL}\delta_{t_i,t_p}\,\delta_{t_k,t_p}\,\delta_{j_i,j_h}$$

$$\xi(l_k+l_h+L)\,\xi(l_i+l_h)\,\widehat{j}_k^2 \left(\begin{array}{ccc} j_k & j_h & L \\ \frac{1}{2} & -\frac{1}{2} & 0 \end{array}\right)^2 \mathcal{J}_L^{[kh];[ik]} \tag{111}$$

$$\sum_{s=\pm 1} s\sqrt{\frac{J+\delta_{s,-1}}{J+\delta_{s,1}}}\,(\chi_p+\chi_h+sJ+\delta_{s,1})\,\mathcal{I}_{J'}^{[pi]}(q)\,,$$

$$T_{3.4;m}^{\mathrm{M(1p1h)}} = -iq\,\frac{G_M^p(q^2)}{2M_p}\,\delta_{t_p,t_h}\,4\pi\,\eta_{ph}^J\,\frac{1}{\widehat{J}^2}\sum_i \delta_{t_i,t_p}\,\delta_{j_i,j_h}\,\xi(l_i+l_h)\,\mathcal{J}_0^{[ih];[\rho]} \tag{112}$$

$$\sum_{s=\pm 1} s\sqrt{\frac{J+\delta_{s,-1}}{J+\delta_{s,1}}}\,(\chi_p+\chi_h+sJ+\delta_{s,1})\mathcal{I}_{J'}^{[pi]}(q)\,,$$

$$T_{3.5;m}^{\mathrm{M(1p1h)}} = -iq\,\frac{G_M^p(q^2)}{2M_p}\,\delta_{t_p,t_h}\,4\pi\,\frac{1}{\widehat{J}^2}\sum_{ikL}\delta_{t_i,t_p}\,\delta_{t_k,t_p}\,(-1)^{j_i+j_k+J+1}\,\eta_{ik}^J\,\frac{1}{\widehat{L}^2}$$

$$\gamma_{pi}^L\,\gamma_{kh}^L \left\{\begin{array}{ccc} j_p & j_h & J \\ j_k & j_i & L \end{array}\right\} \left(\begin{array}{ccc} j_i & j_k & L \\ \frac{1}{2} & -\frac{1}{2} & 0 \end{array}\right) \mathcal{J}_L^{[pi];[kh]} \tag{113}$$

$$\sum_{s=\pm 1} s\sqrt{\frac{J+\delta_{s,-1}}{J+\delta_{s,1}}}\,(\chi_i+\chi_k+sJ+\delta_{s,1})\,\mathcal{I}_{J'}^{[ik]}(q)\,,$$

$$T_{3.6;m}^{\mathrm{M(1p1h)}} = 0\,. \tag{114}$$

In the previous equations we have defined

$$\eta_{\alpha\beta}^\lambda = \frac{1}{\sqrt{4\pi}}\,(-1)^{j_\beta+\lambda-\frac{1}{2}}\,\xi(l_\alpha+l_\beta+\lambda+1)\,\widehat{j}_\alpha\widehat{j}_\beta\widehat{\lambda}\left(\begin{array}{ccc} j_\alpha & j_\beta & \lambda \\ \frac{1}{2} & -\frac{1}{2} & 0 \end{array}\right)\,,$$

and J' stands for $J+s$.

Finally, for the transverse electric and magnetic parts of the convection current contributing to the one-point diagram we have:

$$T_{1;c}^{\mathrm{E(1p1h)}} = \frac{1}{q}\,\frac{G_E^p(q^2)}{2M_p}\,\delta_{t_p,t_h}\,\gamma_{ph}^J\,\frac{1}{\sqrt{J(J+1)}}$$

$$\Big\{[(\chi_p-\chi_h)(\chi_p+\chi_h+1)+J(J+1)]\,\mathcal{I}_J^{[\frac{1}{r}ph']}(q)+ \tag{115}$$

$$[(\chi_p-\chi_h)(\chi_p+\chi_h+1)-J(J+1)]\,\mathcal{I}_J^{[\frac{1}{r}p'h]}(q)\Big\}\,,$$

$$T_{1;c}^{\mathrm{M(1p1h)}} = -i\,\frac{G_E^p(q^2)}{2M_p}\,\delta_{t_p,t_h}\,\eta_{ph}^J\,\frac{(\chi_p+\chi_h)(\chi_p+\chi_h+1)-J(J+1)}{\sqrt{J(J+1)}}\,\mathcal{I}_J^{[\frac{1}{r}ph]}(q)\,, \tag{116}$$

where we have used the following definitions:

$$\mathcal{I}_J^{[\frac{1}{r}ph']}(q) = \int \mathrm{d}r\,r\,j_J(qr)\,R_p^*(r)\,\frac{\mathrm{d}R_h(r)}{\mathrm{d}r}\,, \tag{117}$$

$$\mathcal{I}_J^{[\frac{1}{r}p'h]}(q) = \int \mathrm{d}r\,r\,j_J(qr)\,\frac{\mathrm{d}R_p^*(r)}{\mathrm{d}r}\,R_h(r)\,, \tag{118}$$

$$\mathcal{I}_J^{[\frac{1}{r}ph]}(q) = \int \mathrm{d}r\,r\,j_J(qr)\,R_p^*(r)\,R_h(r)\,. \tag{119}$$

Appendix B. Two-particle emission matrix elements

In this appendix we present the expressions of the matrix elements involved in the two-nucleon emission part of the longitudinal and transverse responses. The charge operator contributes to the first one and the corresponding Coulomb matrix elements are:

$$
\begin{aligned}
M_{2.1}^{(2\mathrm{p}2\mathrm{h})} &= G_E^{p_1}(q^2)\,\delta_{t_{p_1},t_{h_1}}\,\delta_{t_{p_2},t_{h_2}}\,\sqrt{4\pi}\,(-1)^J\,\widehat{J}_p\,\widehat{J}_h\,\widehat{J}\sum_{LK}\frac{\widehat{K}}{\widehat{L}}\,\gamma_{p_1h_1}^K\,\gamma_{p_2h_2}^L \\
&\quad \left\{\begin{array}{ccc} j_{p_1} & j_{p_2} & J_p \\ j_{h_1} & j_{h_2} & J_h \\ K & L & J \end{array}\right\}\left(\begin{array}{ccc} J & K & L \\ 0 & 0 & 0 \end{array}\right)\mathcal{I}_{JL}^{[p_1h_1];[p_2h_2]}(q)\,,
\end{aligned}
\tag{120}
$$

$$
\begin{aligned}
M_{3.1}^{(2\mathrm{p}2\mathrm{h})} &= G_E^{p_1}(q^2)\,\delta_{t_{p_1},t_{h_1}}\,\delta_{t_{p_2},t_{h_2}}\,4\pi\,(-1)^{J+j_{p_1}+j_{h_1}+1}\,\widehat{J}_p\,\widehat{J}_h\sum_{iL}\delta_{t_i,t_{p_1}}\,\frac{1}{\widehat{L}^2} \\
&\quad \gamma_{p_1i}^J\,\gamma_{p_2h_2}^L\,\gamma_{ih_1}^L\left\{\begin{array}{ccc} j_{p_2} & j_{h_2} & L \\ j_{h_1} & j_i & J_h \end{array}\right\}\left\{\begin{array}{ccc} J_p & J_h & J \\ j_i & j_{p_1} & j_{p_2} \end{array}\right\}\mathcal{I}_J^{[p_1i]}(q)\,\mathcal{J}_L^{[p_2h_2];[ih_1]}\,,
\end{aligned}
\tag{121}
$$

$$
\begin{aligned}
M_{3.5}^{(2\mathrm{p}2\mathrm{h})} &= G_E^{p_2}(q^2)\,\delta_{t_{p_1},t_{h_1}}\,\delta_{t_{p_2},t_{h_2}}\,4\pi\,(-1)^{J+j_{p_2}+j_{h_2}+1}\,\widehat{J}_p\,\widehat{J}_h\sum_{iL}\delta_{t_i,t_{p_2}}\,\frac{1}{\widehat{L}^2} \\
&\quad \gamma_{ih_2}^J\,\gamma_{p_2i}^L\,\gamma_{p_1h_1}^L\left\{\begin{array}{ccc} j_{h_1} & j_{p_1} & L \\ j_{p_2} & j_i & J_p \end{array}\right\}\left\{\begin{array}{ccc} J_h & J_p & J \\ j_i & j_{h_2} & j_{h_1} \end{array}\right\}\mathcal{I}_J^{[ih_2]}(q)\,\mathcal{J}_L^{[p_1h_1];[p_2i]}\,,
\end{aligned}
\tag{122}
$$

$$
\begin{aligned}
M_{3.9}^{(2\mathrm{p}2\mathrm{h})} &= G_E^{p_1}(q^2)\,\delta_{t_{p_1},t_{h_2}}\,\delta_{t_{p_2},t_{h_1}}\,\delta_{j_{p_2},j_{h_1}}\,4\pi\,(-1)^{J+j_{p_1}+j_{h_1}}\,\widehat{J}_p\,\widehat{J}_h\,\frac{1}{\widehat{j_{h_1}}^2}\,\gamma_{p_1h_2}^J \\
&\quad \left\{\begin{array}{ccc} J_h & J & J_p \\ j_{p_1} & j_{p_2} & j_{h_2} \end{array}\right\}\mathcal{I}_J^{[p_1h_2]}(q)\sum_{iL}\delta_{t_i,t_{p_2}}\,(-1)^{j_i+j_{h_2}}\,\frac{1}{\widehat{L}^2}\,\gamma_{ih_1}^L\,\gamma_{p_2i}^L\,\mathcal{J}_L^{[p_2i];[ih_1]}\,,
\end{aligned}
\tag{123}
$$

$$
\begin{aligned}
M_{3.11}^{(2\mathrm{p}2\mathrm{h})} &= G_E^{p_1}(q^2)\,\delta_{t_{p_1},t_{h_2}}\,\delta_{t_{p_2},t_{h_1}}\,\delta_{j_{p_2},j_{h_1}}\,4\pi\,(-1)^{J+j_{p_1}+j_{h_2}+1}\,\xi(l_{p_2}+l_{h_1})\,\widehat{J}_p\widehat{J}_h \\
&\quad \gamma_{p_1h_2}^J\left\{\begin{array}{ccc} J_h & J & J_p \\ j_{p_1} & j_{h_1} & j_{h_2} \end{array}\right\}\mathcal{I}_J^{[p_1h_2]}(q)\,\mathcal{J}_0^{[p_2h_1];[\rho]}\,.
\end{aligned}
\tag{124}
$$

As already stated, in our model, the convection current is considered only in the uncorrelated diagrams which do not appear in this case. As a consequence, only the magnetization current contributes to the electric and magnetic transverse terms. For the electric ones, the corresponding matrix elements can be written as follows:

$$
\begin{aligned}
T_{2.1;m}^{\mathrm{E}(2\mathrm{p}2\mathrm{h})} &= q\,\frac{G_M^{p_1}(q^2)}{2M_{p_1}}\,\delta_{t_{p_1},t_{h_1}}\,\delta_{t_{p_2},t_{h_2}}\,\sqrt{12}\,(-1)^{J+l_{h_1}}\,\widehat{J}_p\,\widehat{J}_h\,\widehat{J}\,\widehat{j}_{p_1}\,\widehat{j}_{h_1}\,\widehat{l}_{p_1}\,\widehat{l}_{h_1} \\
&\quad \sum_L\frac{1}{\widehat{L}}\,\gamma_{p_2h_2}^L\,\mathcal{I}_{JL}^{[p_1h_1];[p_2h_2]}(q)\sum_K\widehat{K}^2\left(\begin{array}{ccc} K & J & L \\ 1 & -1 & 0 \end{array}\right)\left\{\begin{array}{ccc} j_{p_1} & j_{p_2} & J_p \\ j_{h_1} & j_{h_2} & J_h \\ K & L & J \end{array}\right\} \\
&\quad \sum_\lambda\widehat{\lambda}^2\,\xi(L+J+\lambda)\left(\begin{array}{ccc} l_{p_1} & \lambda & l_{h_1} \\ 0 & 0 & 0 \end{array}\right)\left(\begin{array}{ccc} 1 & K & \lambda \\ 1 & -1 & 0 \end{array}\right)\left\{\begin{array}{ccc} l_{p_1} & \frac{1}{2} & j_{p_1} \\ l_{h_1} & \frac{1}{2} & j_{h_1} \\ \lambda & 1 & K \end{array}\right\}\,,
\end{aligned}
\tag{125}
$$

$$
T_{3.1;m}^{\mathrm{E}(2\mathrm{p}2\mathrm{h})} = q\,\frac{G_M^{p_1}(q^2)}{2M_{p_1}}\,\delta_{t_{p_1},t_{h_1}}\,\delta_{t_{p_2},t_{h_2}}\,\sqrt{4\pi}\,(-)^{J+j_{p_1}+j_{h_1}+l_{p_1}+1}\,\widehat{J}_p\,\widehat{J}_h\,\widehat{J}\,\widehat{j}_{p_1}
\tag{126}
$$

$$\sum_{iL} \delta_{t_i,t_{p_1}}\, \xi(l_{p_1}+l_i+J)\, \frac{\widehat{j}_i}{\widehat{L}^2}\, \gamma^L_{ih_1}\, \gamma^L_{p_2h_2}\, \mathcal{I}^{[p_1 i]}_J(q) \mathcal{J}^{[p_2h_2];[ih_1]}_L$$
$$\left\{ \begin{array}{ccc} J_p & J_h & J \\ j_i & j_{p_1} & j_{p_2} \end{array} \right\} \left\{ \begin{array}{ccc} j_{p_2} & j_{h_2} & L \\ j_{h_1} & j_i & J_h \end{array} \right\} \left(\begin{array}{ccc} j_i & j_{p_1} & J \\ -\frac{1}{2} & -\frac{1}{2} & 1 \end{array} \right),$$

$$\begin{aligned} T^{\mathrm{E(2p2h)}}_{3.5;m} &= q\, \frac{G^{p_2}_M(q^2)}{2M_{p_2}}\, \delta_{t_{p_1},t_{h_1}}\, \delta_{t_{p_2},t_{h_2}}\, \sqrt{4\pi}\, (-1)^{J+j_{p_2}+j_{h_2}+1}\, \widehat{J}_p\, \widehat{J}_h\, \widehat{J}\,\widehat{j}_{h_2} \\ & \sum_{iL} \delta_{t_i,t_{p_2}}\, (-1)^{l_i}\, \xi(l_i+l_{h_2}+J)\, \frac{\widehat{j}_i}{\widehat{L}^2}\, \gamma^L_{p_2 i}\, \gamma^L_{p_1h_1}\, \mathcal{I}^{[ih_2]}_J(q)\, \mathcal{J}^{[p_2 i];[p_1h_1]}_L \\ & \left\{ \begin{array}{ccc} J_h & J_p & J \\ j_i & j_{h_2} & j_{h_1} \end{array} \right\} \left\{ \begin{array}{ccc} j_{h_1} & j_{p_1} & L \\ j_{p_2} & j_i & J_p \end{array} \right\} \left(\begin{array}{ccc} j_{h_2} & j_i & J \\ -\frac{1}{2} & -\frac{1}{2} & 1 \end{array} \right), \end{aligned} \tag{127}$$

$$\begin{aligned} T^{\mathrm{E(2p2h)}}_{3.9;m} &= q\, \frac{G^{p_1}_M(q^2)}{2M_{p_1}}\, \delta_{t_{p_1},t_{h_2}}\, \delta_{t_{p_2},t_{h_1}}\, \delta_{j_{p_2},j_{h_1}}\, \sqrt{4\pi}\, (-1)^{J+j_{p_1}+j_{h_1}+l_{p_1}} \\ & \xi(l_{p_1}+l_{h_2}+J)\, \widehat{J}_p\, \widehat{J}_h\, \widehat{J}\,\widehat{j}_{p_1}\, \frac{\widehat{j}_{h_2}}{\widehat{j}^2_{p_2}} \left\{ \begin{array}{ccc} J_h & J & J_p \\ j_{p_1} & j_{p_2} & j_{h_2} \end{array} \right\} \left(\begin{array}{ccc} j_{h_2} & j_{p_1} & J \\ -\frac{1}{2} & -\frac{1}{2} & 1 \end{array} \right) \mathcal{I}^{[p_1h_2]}_J(q) \\ & \sum_{iL} \delta_{t_i,t_{p_2}}\, (-1)^{j_i+j_{h_2}}\, \frac{1}{\widehat{L}^2}\, \gamma^L_{ih_1}\, \gamma^L_{p_2 i}\, \mathcal{J}^{[p_2 i];[ih_1]}_L, \end{aligned} \tag{128}$$

$$\begin{aligned} T^{\mathrm{E(2p2h)}}_{3.11;m} &= q\, \frac{G^{p_1}_M(q^2)}{2M_{p_1}}\, \delta_{t_{p_1},t_{h_2}}\, \delta_{t_{p_2}t_{h_1}}\, \delta_{j_{p_2},j_{h_1}}\, \sqrt{4\pi}\, (-1)^{J+j_{p_1}+j_{h_2}+l_{p_1}+1} \\ & \xi(l_{p_1}+l_{h_2}+J)\, \xi(l_{p_2}+l_{h_1})\, \widehat{J}_p\, \widehat{J}_h\, \widehat{J}\widehat{j}_{p_1}\, \widehat{j}_{h_2} \\ & \left\{ \begin{array}{ccc} J_h & J & J_p \\ j_{p_1} & j_{h_1} & j_{h_2} \end{array} \right\} \left(\begin{array}{ccc} j_{h_2} & j_{p_1} & J \\ -\frac{1}{2} & -\frac{1}{2} & 1 \end{array} \right) \mathcal{I}^{[p_1h_2]}_J(q)\, \mathcal{J}^{[p_2h_1];[\rho]}_0. \end{aligned} \tag{129}$$

Finally, the magnetic transverse matrix elements of the magnetization current are:

$$\begin{aligned} T^{\mathrm{M(2p2h)}}_{2.1;m} &= iq\, \frac{G^{p_1}_M(q^2)}{2M_{p_1}}\, \delta_{t_{p_1},t_{h_1}}\, \delta_{t_{p_2},t_{h_2}}\, \sqrt{6}\, (-1)^{l_{p_1}}\, \widehat{J}_p\, \widehat{J}_h\, \widehat{j}_{p_1}\, \widehat{j}_{h_1} \widehat{l}_{p_1}\, \widehat{l}_{h_1} \\ & \sum_{LK} (-1)^{K+L}\, \frac{\widehat{K}^2}{\widehat{L}}\, \gamma^L_{p_2h_2} \left\{ \begin{array}{ccc} j_{p_1} & j_{p_2} & J_p \\ j_{h_1} & j_{h_2} & J_h \\ K & L & J \end{array} \right\} \sum_s s\, \sqrt{J+\delta_{s,-1}}\, \widehat{J}'\, \mathcal{I}^{[p_1h_1];[p_2h_2]}_{J'L}(q) \\ & \sum_\lambda \widehat{\lambda}^2 \left\{ \begin{array}{ccc} l_{p_1} & \frac{1}{2} & j_{p_1} \\ l_{h_1} & \frac{1}{2} & j_{h_1} \\ \lambda & 1 & K \end{array} \right\} \left(\begin{array}{ccc} l_{p_1} & \lambda & l_{h_1} \\ 0 & 0 & 0 \end{array} \right) \left\{ \begin{array}{ccc} L & J' & \lambda \\ 1 & K & J \end{array} \right\} \left(\begin{array}{ccc} L & J' & \lambda \\ 0 & 0 & 0 \end{array} \right), \end{aligned} \tag{130}$$

$$\begin{aligned} T^{\mathrm{M(2p2h)}}_{3.1;m} &= iq\, \frac{G^{p_1}_M(q^2)}{2M_{p_1}}\, \delta_{t_{p_1},t_{h_1}}\, \delta_{t_{p_2},t_{h_2}}\, 4\pi\, (-1)^{j_{p_1}+j_{h_1}+J}\, \frac{\widehat{J}_p\widehat{J}_h}{\widehat{J}^2} \sum_{iL} \delta_{t_i,t_{p_1}}\, \frac{1}{\widehat{L}^2}\, \eta^J_{p_1 i} \\ & \left\{ \begin{array}{ccc} j_{p_2} & j_{h_2} & L \\ j_{h_1} & j_i & J_h \end{array} \right\} \left\{ \begin{array}{ccc} J_p & J_h & J \\ j_i & j_{p_1} & j_{p_2} \end{array} \right\} \gamma^L_{ih_1}\, \gamma^L_{p_2h_2}\, \mathcal{J}^{[ih_1];[p_2h_2]}_L \\ & \sum_s s\, \sqrt{\frac{J+\delta_{s,-1}}{J+\delta_{s,1}}}\, (\chi_{p_1}+\chi_i+sJ+\delta_{s,1})\, \mathcal{I}^{[p_1 i]}_{J'}(q), \end{aligned} \tag{131}$$

$$
\begin{aligned}
T^{\mathrm{M(2p2h)}}_{3.5;m} \;=\;& iq\,\frac{G_M^{h_2}(q^2)}{2M_{h_2}}\,\delta_{t_{p_1},t_{h_1}}\,\delta_{t_{p_2},t_{h_2}}\,4\pi\,(-1)^{j_{h_2}+j_{p_2}+J}\,\frac{\widehat{J}_p\widehat{J}_h}{\widehat{J}^2}\sum_{iL}\delta_{t_i,t_{p_2}}\,\frac{1}{\widehat{L}^2}\,\eta^J_{ih_2} \\
&\left\{\begin{array}{ccc} j_{h_1} & j_{p_1} & L \\ j_{p_2} & j_i & J_p \end{array}\right\}\left\{\begin{array}{ccc} J_h & J_p & J \\ j_i & j_{h_2} & j_{h_1} \end{array}\right\}\gamma^L_{p_1h_1}\gamma^L_{p_2i}\,\mathcal{J}_L^{[p_2i];[p_1h_1]} \\
&\sum_s s\sqrt{\frac{J+\delta_{s,-1}}{J+\delta_{s,1}}}\,(\chi_{h_2}+\chi_i+sJ+\delta_{s,1})\,\mathcal{I}^{[ih_2]}_{J'}(q)\,,
\end{aligned}
\tag{132}
$$

$$
\begin{aligned}
T^{\mathrm{M(2p2h)}}_{3.9;m} \;=\;& -iq\,\frac{G_M^{p_1}(q^2)}{2M_{p_1}}\,\delta_{t_{p_1},t_{h_2}}\,\delta_{t_{p_2},t_{h_1}}\,\delta_{j_{h_1},j_{p_2}}\,4\pi\,(-1)^{J+j_{p_1}+j_{h_1}}\,\frac{\widehat{J}_p\widehat{J}_h}{\widehat{J}^2\widehat{j}^2_{h_1}}\,\eta^J_{p_1h_2} \\
&\left\{\begin{array}{ccc} J_h & J & J_p \\ j_{p_1} & j_{p_2} & j_{h_2} \end{array}\right\}\sum_s s\sqrt{\frac{J+\delta_{s,-1}}{J+\delta_{s,1}}}\,(\chi_{p_1}+\chi_{h_2}+sJ+\delta_{s,1})\,\mathcal{I}^{[p_1h_2]}_{J'}(q) \\
&\sum_{iL}\delta_{t_i,t_{p_2}}\,(-1)^{j_i+j_{h_2}}\,\frac{1}{\widehat{L}^2}\,\gamma^L_{ih_1}\,\gamma^L_{p_2i}\,\mathcal{J}_L^{[p_2i];[ih_1]}\,,
\end{aligned}
\tag{133}
$$

$$
\begin{aligned}
T^{\mathrm{M(2p2h)}}_{3.11;m} \;=\;& iq\,\frac{G_M^{p_1}(q^2)}{2M_{p_1}}\,\delta_{t_{p_1},t_{h_2}}\,\delta_{t_{p_2},t_{h_1}}\,\delta_{j_{p_2},j_{h_1}}\,4\pi\,(-1)^{J+j_{p_1}+j_{h_2}}\,\xi(l_{p_2}+l_{h_1})\,\frac{\widehat{J}_p\widehat{J}_h}{\widehat{J}^2}\,\eta^J_{p_1h_2} \\
&\left\{\begin{array}{ccc} J_h & J & J_p \\ j_{p_1} & j_{h_1} & j_{h_2} \end{array}\right\}\mathcal{J}_0^{[p_2h_1];[\rho]}\,\sum_s s\sqrt{\frac{J+\delta_{s,-1}}{J+\delta_{s,1}}}\,(\chi_{p_1}+\chi_{h_2}+sJ+\delta_{s,1})\,\mathcal{I}^{[p_1h_2]}_{J'}(q)\,.
\end{aligned}
\tag{134}
$$

The integrals and symbols used in these equations are defined in Appendix A.

References

[1] C. R. Chen, G. L. Payne, J. L. Friar and B. F. Gibson, *Phys. Rev. C* **33** (1986), 1740.

[2] A. Stadler, W. Glöckle and P. U. Sauer, *Phys. Rev. C* **44** (1991), 2319.

[3] A. Kievsky, M. Viviani and S. Rosati, *Nucl. Phys. A* **551** (1993), 241.

[4] V.D. Efros, W. Leidemann, G. Orlandini and E.L. Tomusiak, LANL e-print archives, nucl-th/9911049.

[5] B. S. Pudliner, V. R. Pandharipande, J. Carlson, S. C. Pieper and R. B. Wiringa, *Phys. Rev. C* **56** (1997), 1720.

[6] S. C. Pieper, R. B. Wiringa and V. R. Pandharipande, *Phys. Rev. C* **46** (1992), 1741.

[7] K.W. Schmid, H. Müther and R. Machleidt, *Nucl. Phys. A* **530** (1991), 14.

[8] J. H. Heisenberg and B. Mihaila, *Phys. Rev. C* **59** (1999), 1440.

[9] A. Fabrocini, F. Arias de Saavedra and G. Co', *Phys. Rev. C* **61** (2000), 044302.

[10] J.W. Clark, *Prog. Part. Nucl. Phys.* **2** (1979) 89; V. R. Pandharipande and R. B. Wiringa, *Rev. Mod. Phys.* **51** (1979), 821. S. Rosati, in *From nuclei to particles*, Proc. Int. School E. Fermi, course LXXIX, ed. A. Molinari (North Holland, Amsterdam, 1982).

[11] R. B. Wiringa, V. Ficks and A. Fabrocini, *Phys. Rev. C* **38** (1988), 1010.

[12] A. Akmal and V. R. Pandharipande, *Phys. Rev. C* **55** (1997), 2261.

[13] A. Akmal, V. R. Pandharipande and D. G. Ravenhall, *Phys. Rev. C* **58** (1988), 1140.

[14] R. B. Wiringa, R. A. Smith and T. L. Ainsworth, *Phys. Rev. C* **29** (1984), 1207.

[15] R. B. Wiringa, V. G. J. Stoks and R. Schiavilla, *Phys. Rev. C* **51**, 38 (1995).

[16] R. Schiavilla, V. R. Pandharipande and R. B. Wiringa, *Nucl. Phys. A* **449** (1986), 219.

[17] S. Fantoni and V. R. Pandharipande, *Nucl. Phys. A* **473** (1987), 234.

[18] A. Fabrocini and S. Fantoni, *Nucl. Phys. A* **503**, 375 (1989); O. Benhar, A. Fabrocini and S. Fantoni, *Nucl. Phys. A* **550**, 201 (1992); A. Fabrocini, *Phys. Rev. C* **55**, 330 (1997).

[19] J.E. Amaro, A.M. Lallena, G. Co' and A. Fabrocini, *Phys. Rev. C* **57** (1998), 3473.

[20] R.D. Smith and J. Wambach, *Phys. Rev. C* **38** (1988), 100.

[21] G. Co', K.Q. Quader, R.D. Smith and J. Wambach, *Nucl. Phys. A* **485** (1988), 61.

[22] A.R. Edmonds, *Angular momentum in quantum mechanics*, Princeton University Press, Princeton, 1957.

[23] F. Arias de Saavedra, G. Co', A. Fabrocini and S. Fantoni, Nucl. Phys. A **605** (1996), 359.

[24] C.W. De Jager and C. De Vries, *At. Data and Nucl. Data Tables*, **36** (1987), 495.

[25] G. Hoehler, E. Pietarinen, I. Sabba-Stefabescu, F. Borkowski, G.G. Simon, V.H. Walther and R.D. Wendling, *Nucl. Phys. B* **114** (1976),505.

[26] J.E. Amaro, G. Co' and A.M. Lallena, *Ann. Phys.* **221** (1993), 306.

[27] G. Co', *Nuov. Cim.* **A108** (1995), 623.

[28] F. Arias de Saavedra, G. Co' and M.M. Renis, *Phys. Rev. C* **55** (1997), 673.

[29] J.E. Amaro, G. Co' and A.M. Lallena, (nucl-th 9902072), to be published.

[30] C. Mahaux and N. Ngô, *Nucl. Phys.* **A378** (1982), 205.

[31] D. Pines, K.Q. Quader and J. Wambach, *Nucl. Phys.* **A477** (1988), 365.

[32] T.C.Yates et al. *Phys Lett.* **B 312** (1993), 382.

[33] C.F.Williamson et al., *Phys. Rev. C* **56** (1997), 3152.

[34] M. Anghinolfi et al., *Nucl. Phys.* A602 (1996), 405.

[35] G.Co' and A.M.Lallena, *Phys. Rev. C* **57** (1998), 145.

[36] A. Fabrocini, *Phys. Rev. C* **55** (1997), 338.

[37] J.E. Amaro, G. Co' and A.M. Lallena, *Nucl. Phys.* A578 (1994), 365.

Table 1: Parameters of the Woods-Saxon potentials used to generate the set of single particle wave functions.

		^{16}O		^{40}Ca	
		V8	S3	V8	S3
π	V_0 [MeV]	-53.0	-52.5	-50.0	-57.5
	V_{ls} [MeV]	0.0	-7.0	0.0	-11.11
	R [fm]	3.45	3.2	4.6	4.1
	a [fm]	0.7	0.53	0.5	0.53
ν	V_0 [MeV]	-53.0	-52.5	-50.0	-55.0
	V_{ls} [MeV]	0.0	-6.54	0.0	-8.5
	R [fm]	3.45	3.2	4.6	4.1
	a [fm]	0.7	0.53	0.5	0.53

Table 2: Single particle energies, in MeV, of the ^{16}O nucleus obtained with the two chosen potentials. We have indicated with π and ν proton and neutron states respectively.

		^{16}O		
		V8	S3	exp
π	1s1/2	-30.7	-30.0	
	1p3/2	-17.6	-16.9	-18.4
	1p1/2	-17.6	-12.7	-12.1
ν	1s1/2	-34.5	-34.0	
	1p3/2	-21.0	-20.5	-21.8
	1p1/2	-21.0	-16.6	-15.7

.

Table 3: Single particle energies, in MeV, of the ^{40}Ca nucleus obtained with the two chosen potentials. We have indicated with π and ν proton and neutron states respectively.

		^{40}Ca		
		V8	S3	exp
π	1s1/2	-32.5	-36.0	
	1p3/2	-24.0	-26.5	
	1p1/2	-24.0	-23.0	
	1d5/2	-14.0	-16.2	-14.7
	1d3/2	-14.0	-8.7	-8.3
	2s1/2	-11.0	-10.3	-10.3
ν	1s1/2	-40.4	-42.6	
	1p3/2	-31.5	-32.4	
	1p1/2	-31.5	-29.8	
	1d5/2	-21.1	-21.4	-18.2
	1d3/2	-21.1	-15.7	-15.6
	2s1/2	-18.2	-16.4	-21.6

Table 4: Parameters used for the correlation given in Eq. (68).

	g1	g2	g3	g4	g5	g6
A	0.8	0.6	0.4	0.8	0.8	0.8
B [fm^{-2}]	2.2	2.0	1.9	2.2	2.2	2.2
C	0.0	0.0	0.0	0.04	0.04	0.04
D [fm^{-2}]	0.0	0.0	0.0	3.0	3.0	3.0
r_0 [fm]	0.0	0.0	0.0	1.5	2.0	2.5

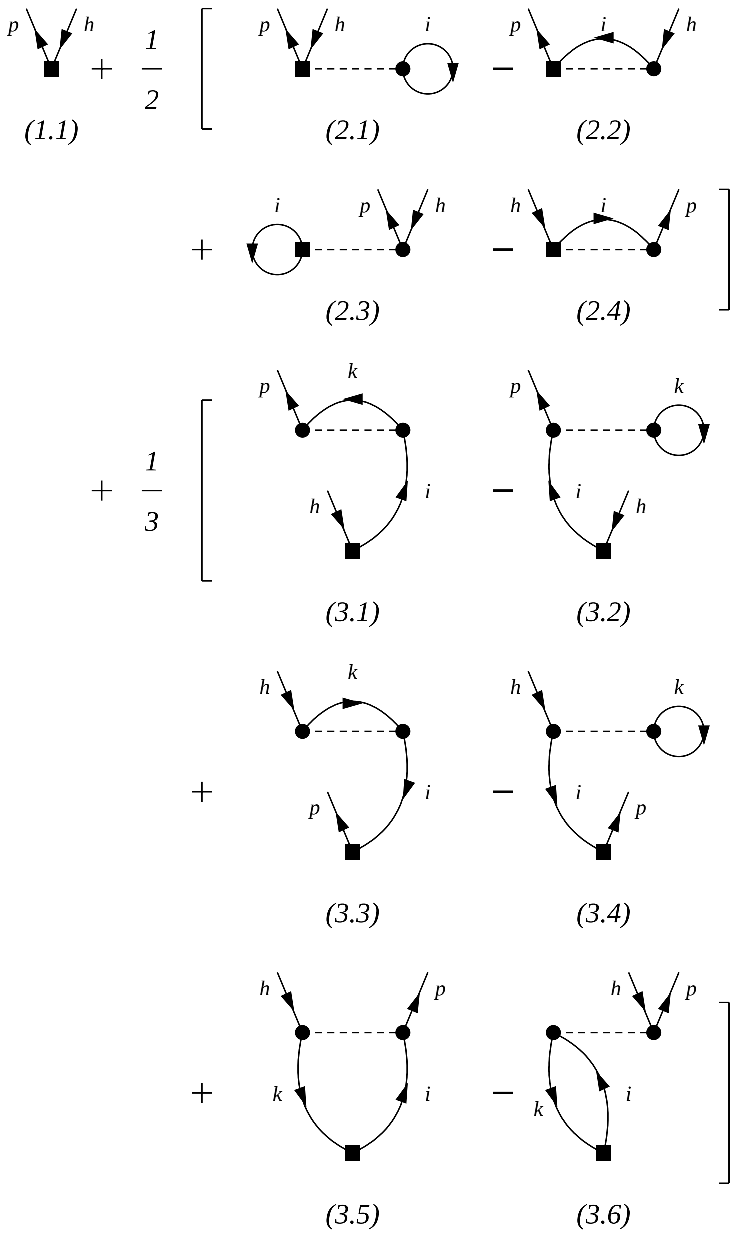

Figure 1: Diagrams considered in the calculation of the one-particle one-hole responses. The dashed lines represent the correlation function h and the continuous oriented lines the single particle wave functions. The letter i, k, h indicates hole wave functions and p particle wave functions. A sum on the i and k indexes is understood. The black squares represent the point where the excitation operator is acting.

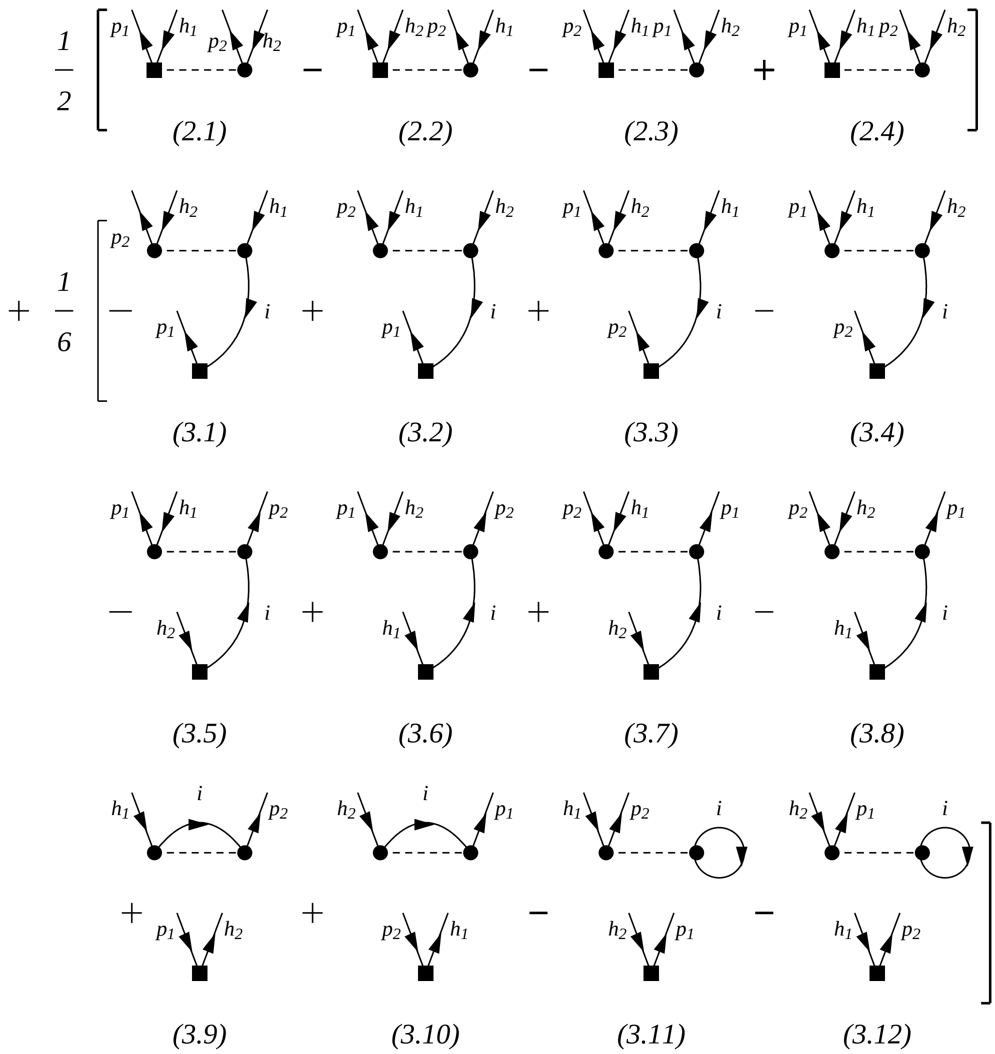

Figure 2: Diagrams considered in the calculation of the two-particle two-hole responses. The symbols have the same meaning as in Fig. 1.

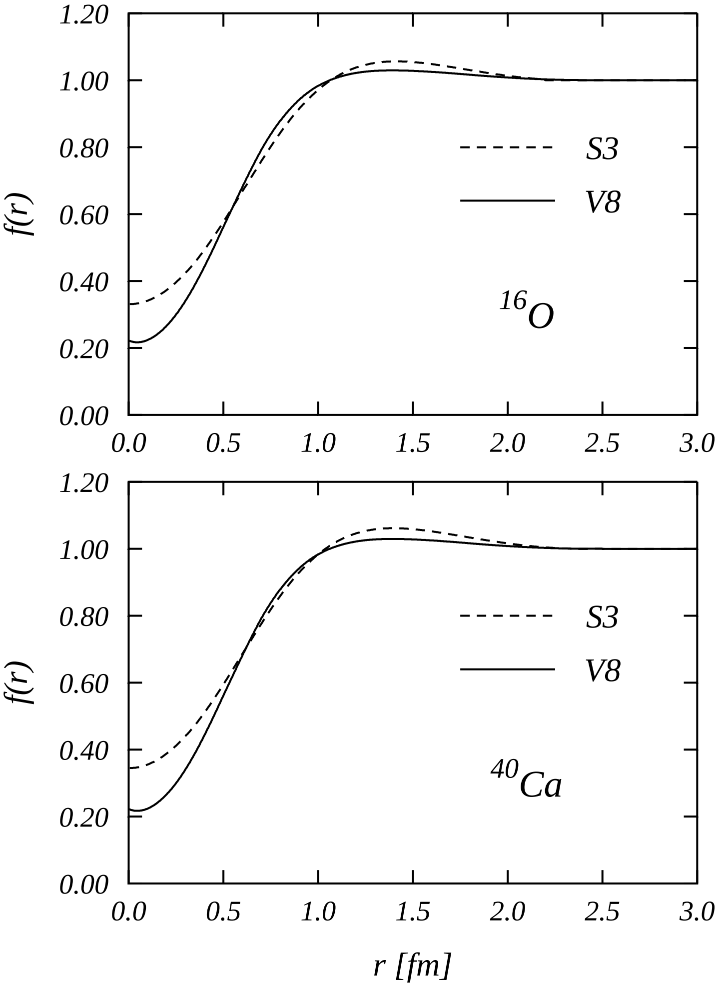

Figure 3: Correlation functions used in the calculations. The label S3 refer to the FHNC calculations of Ref. [23] while V8 to those of Ref. [9].

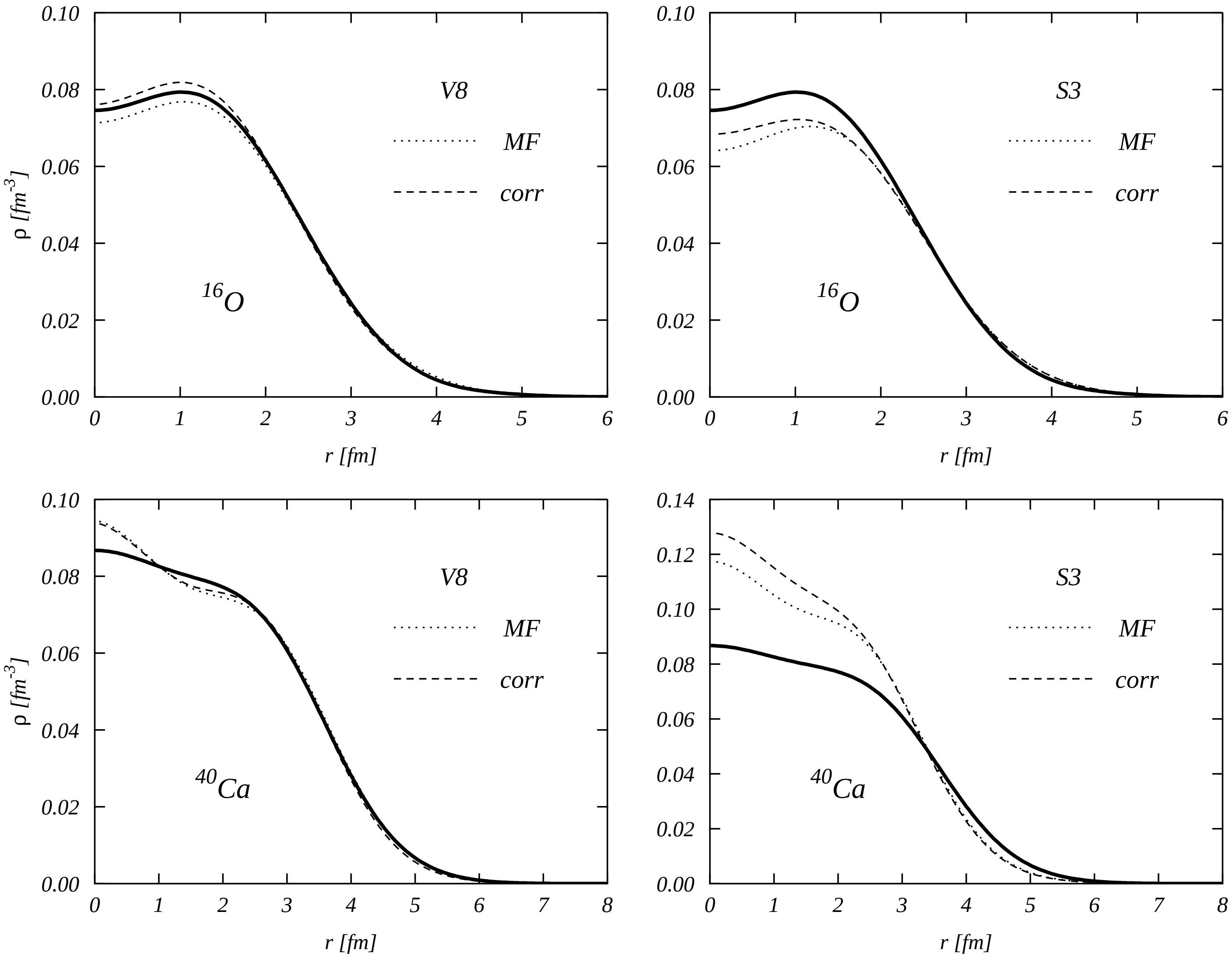

Figure 4: MF (dotted lines) and correlated (dashed lines) charge densities distributions compared with the empirical densities (full lines) taken from the compilation of Ref. [24].

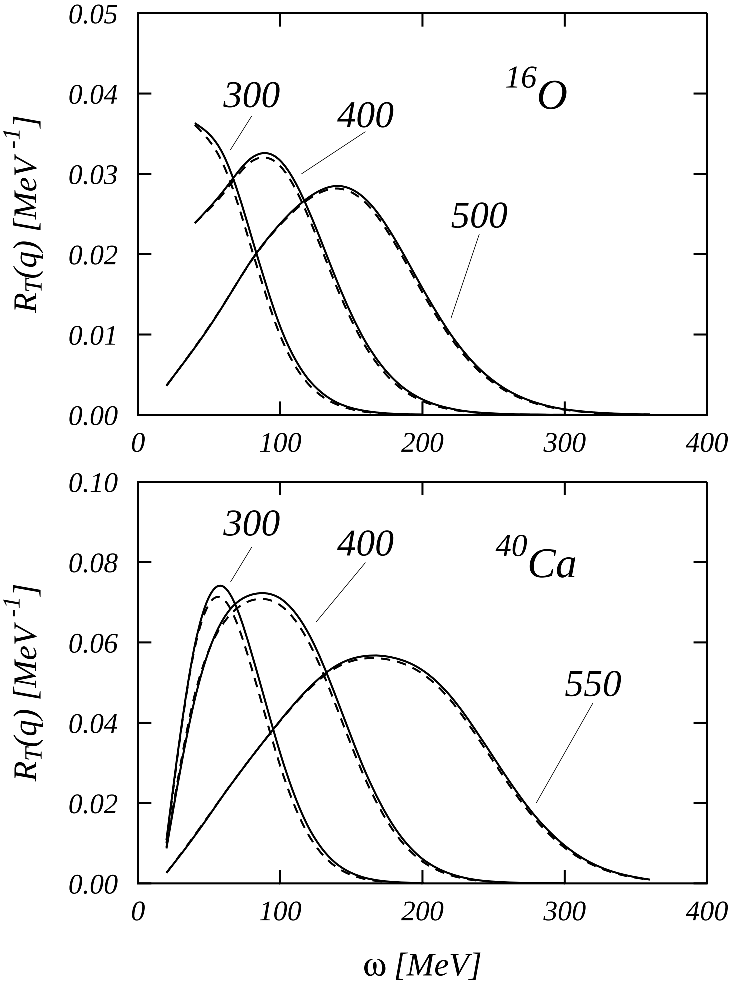

Figure 5: MF transverse responses calculated with the S3 Woods-Saxon potentials considering magnetization current only (dashed lines) and magnetization plus convection current (full lines). The numbers in the figure indicates the values of the momentum transfer in MeV/c units.

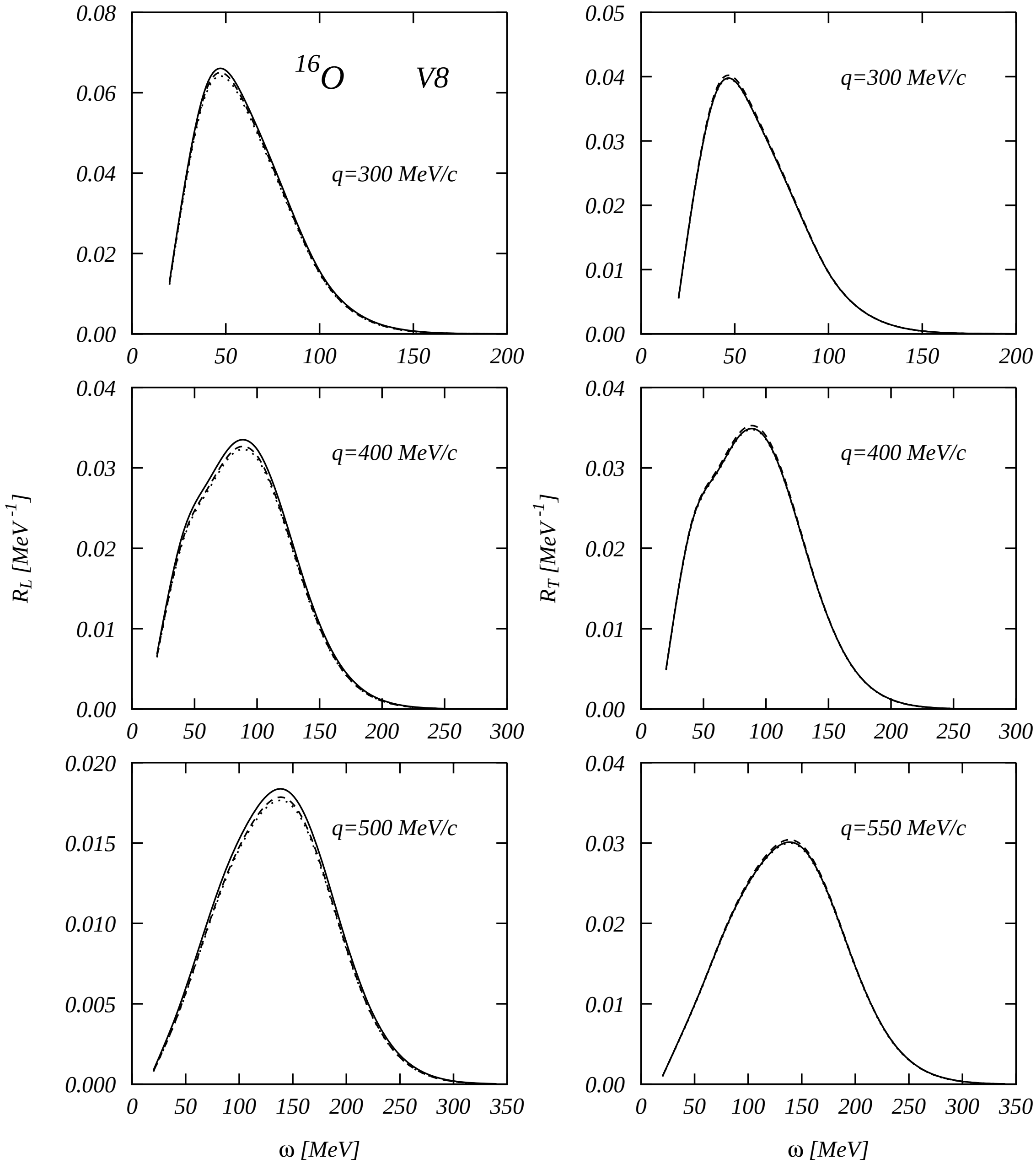

Figure 6: Longitudinal and transverse 1p-1h responses in ^{16}O for three different values of the momentum transfer. The calculations have been done with the V8 wave functions and correlations. The full lines show the MF responses, the dotted lines have been obtained with the inclusion of the two-point diagrams of Fig. 1, while the dashed lines have been obtained considering all the diagrams of that figure.

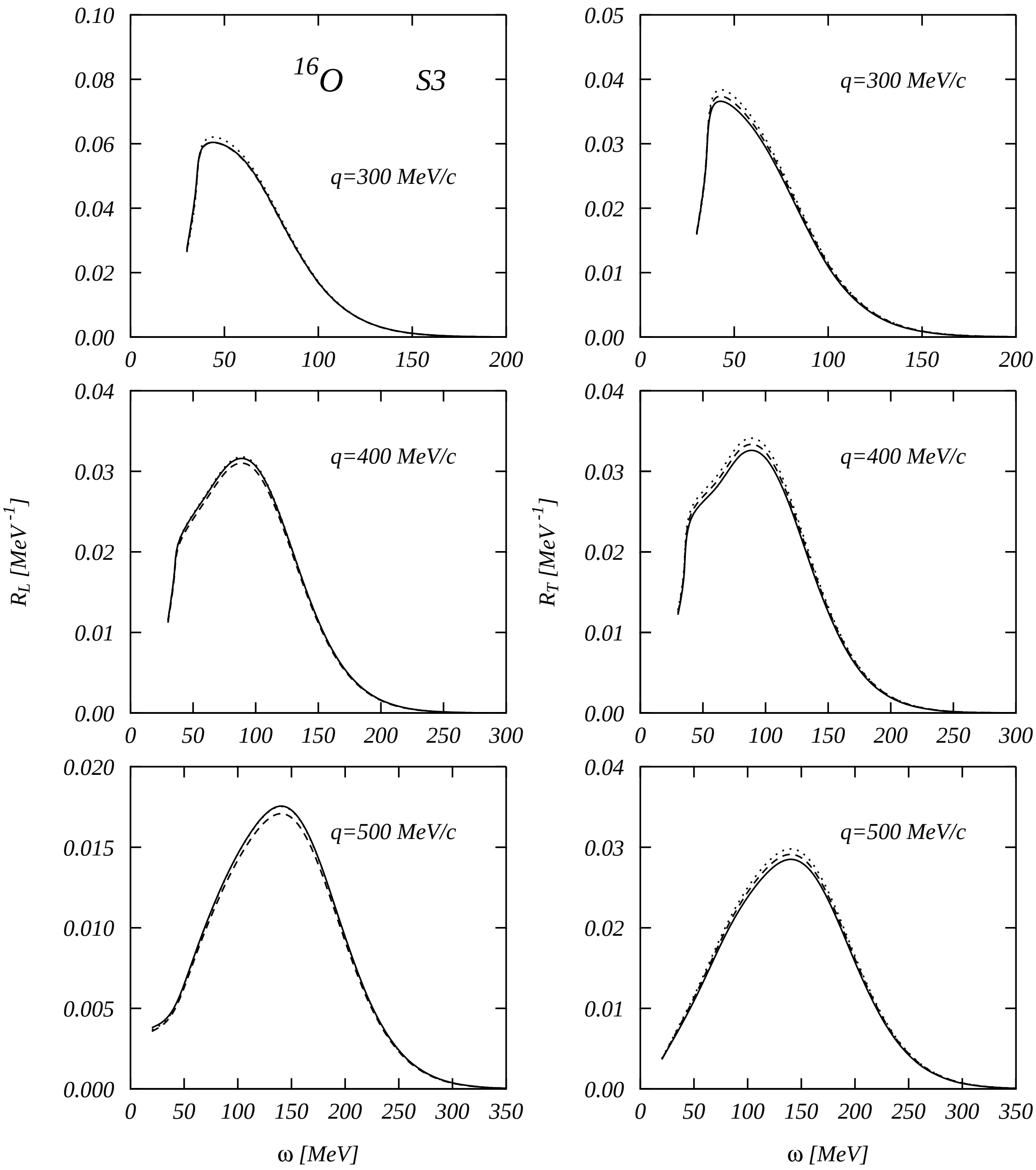

Figure 7: The same as in Fig. 6 with the S3 input.

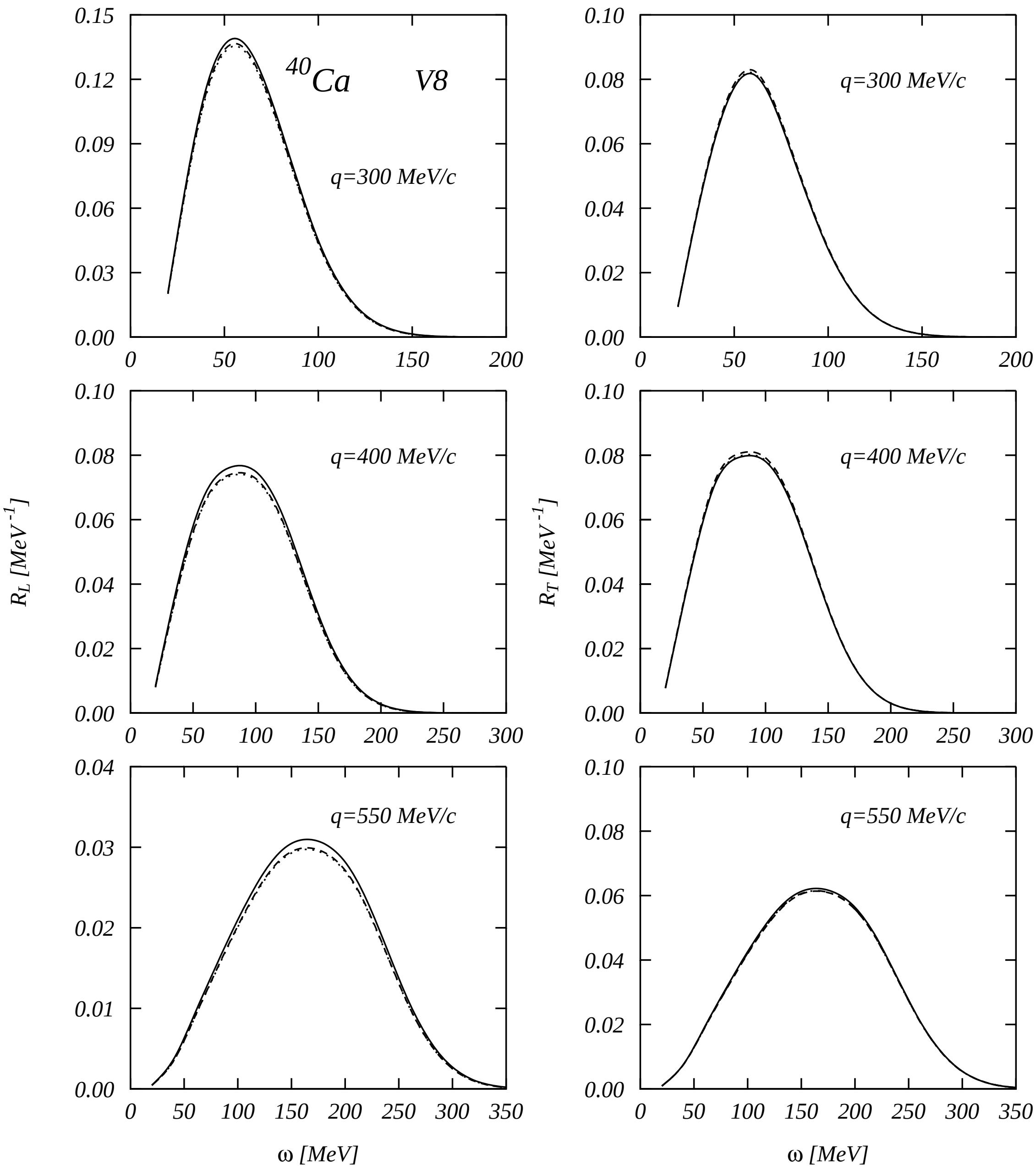

Figure 8: The same as in Fig. 6 for ^{40}Ca.

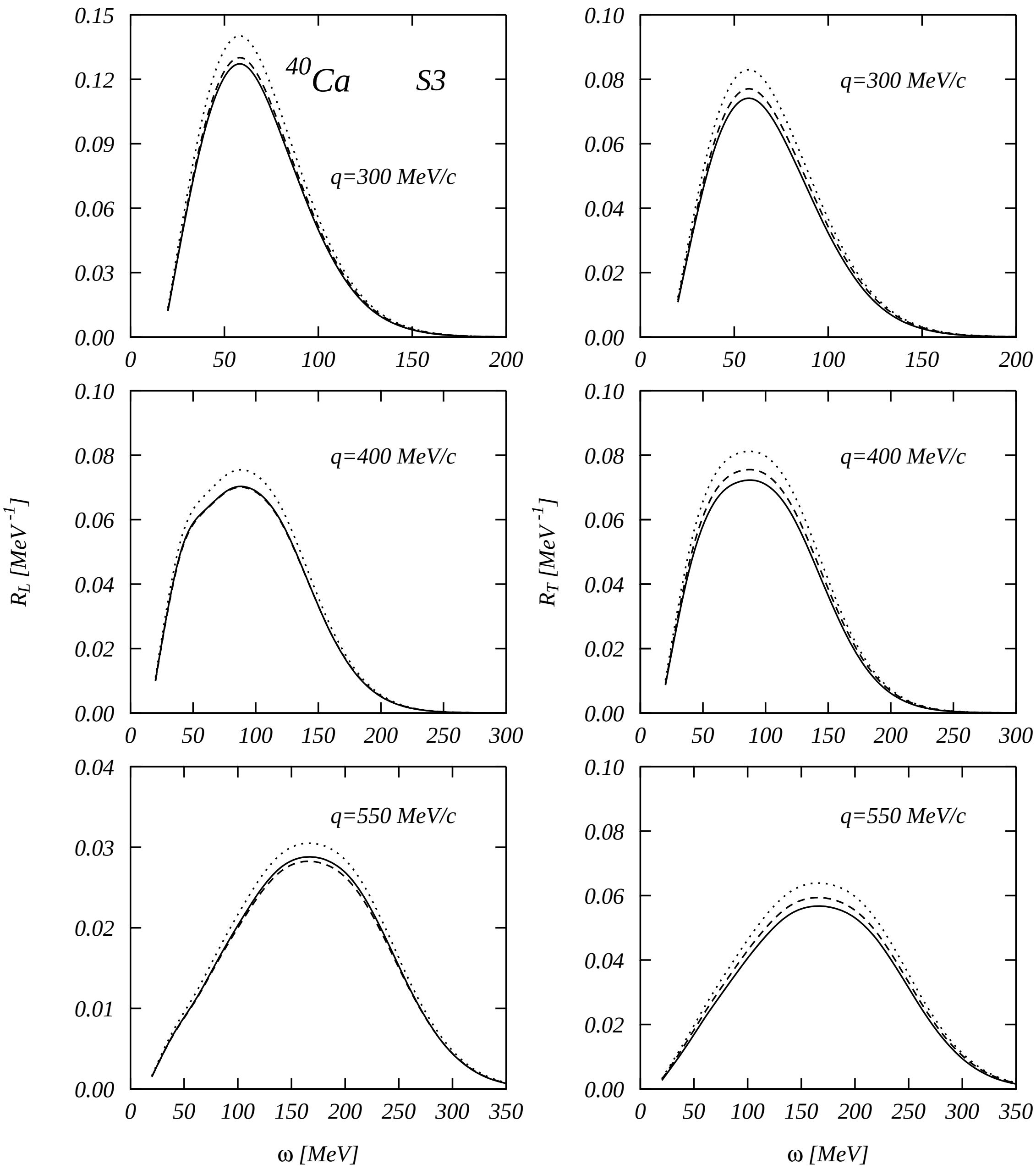

Figure 9: The same as in Fig. 7 for ^{40}Ca.

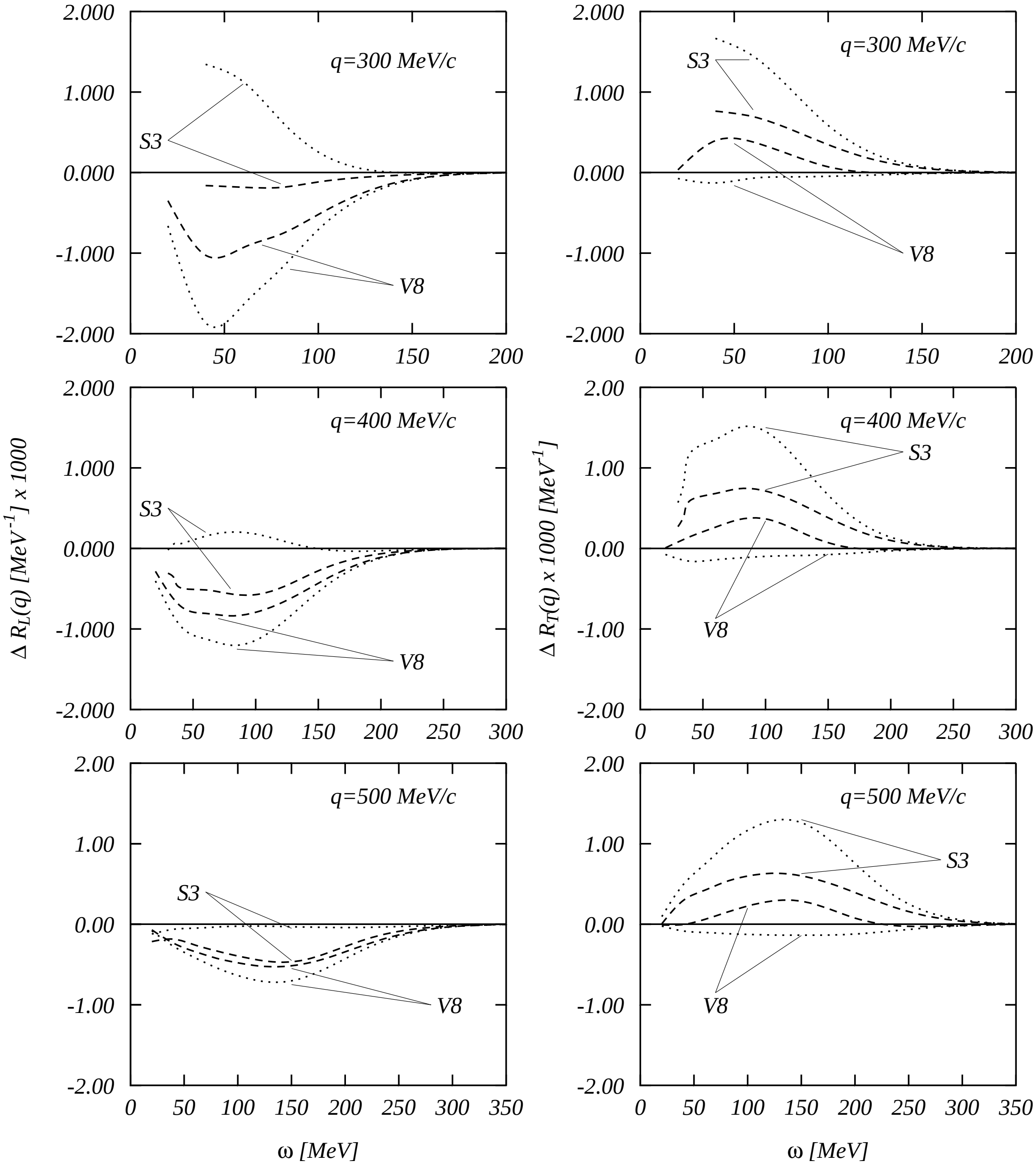

Figure 10: Differences between correlated and MF responses as defined in Eq. (67) for ^{16}O.

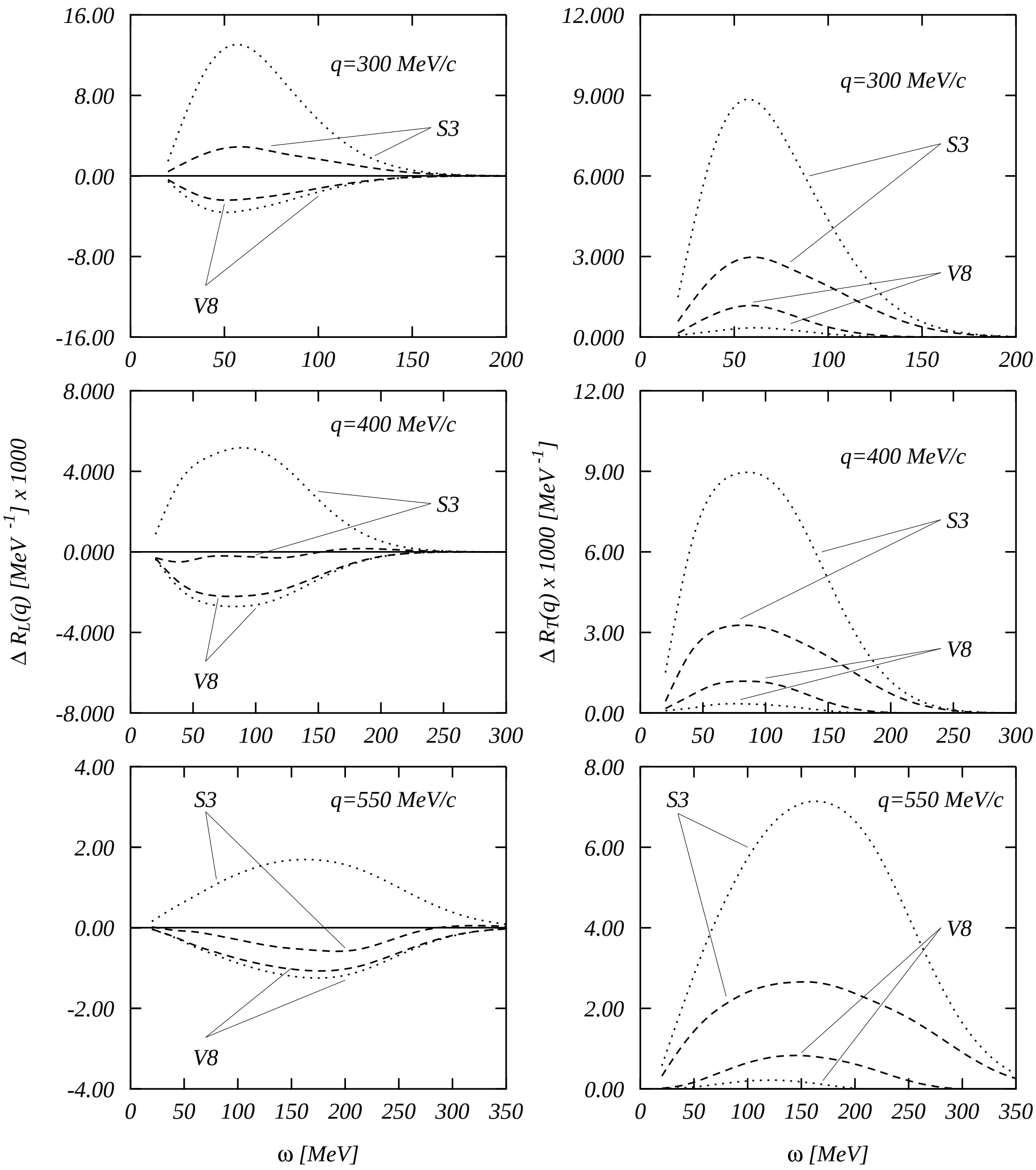

Figure 11: The same as Fig. 10 for ^{40}Ca.

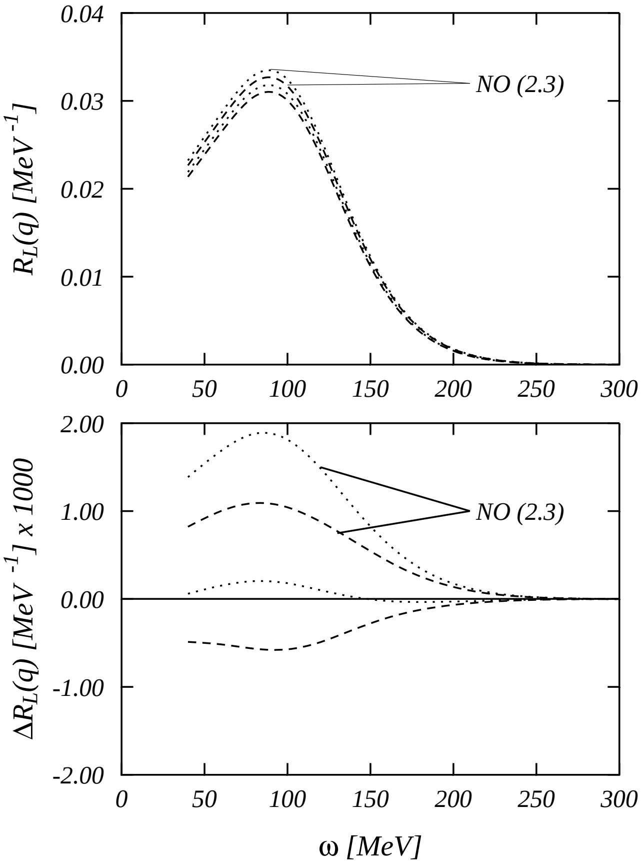

Figure 12: Upper panel: ^{16}O longitudinal responses calculated with the S3 input. The curves indicated with **NO (2.3)** have been obtained without the (2.3) diagram of Fig. 1. The other curves correspond to those shown in Fig. 7. Lower panel: difference between the correlated and MF responses. Also in this figure the dotted lines indicate the results obtained by using only the two-point diagrams, while the dashed lines show the results of the full calculation.

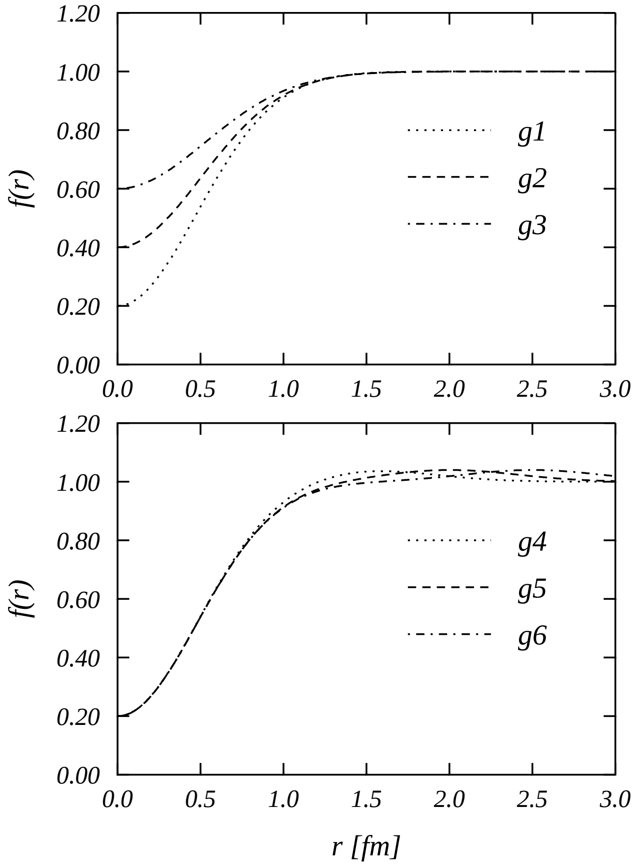

Figure 13: Correlation obtained with the expression (68) for the various parameterizations given in Table 4.

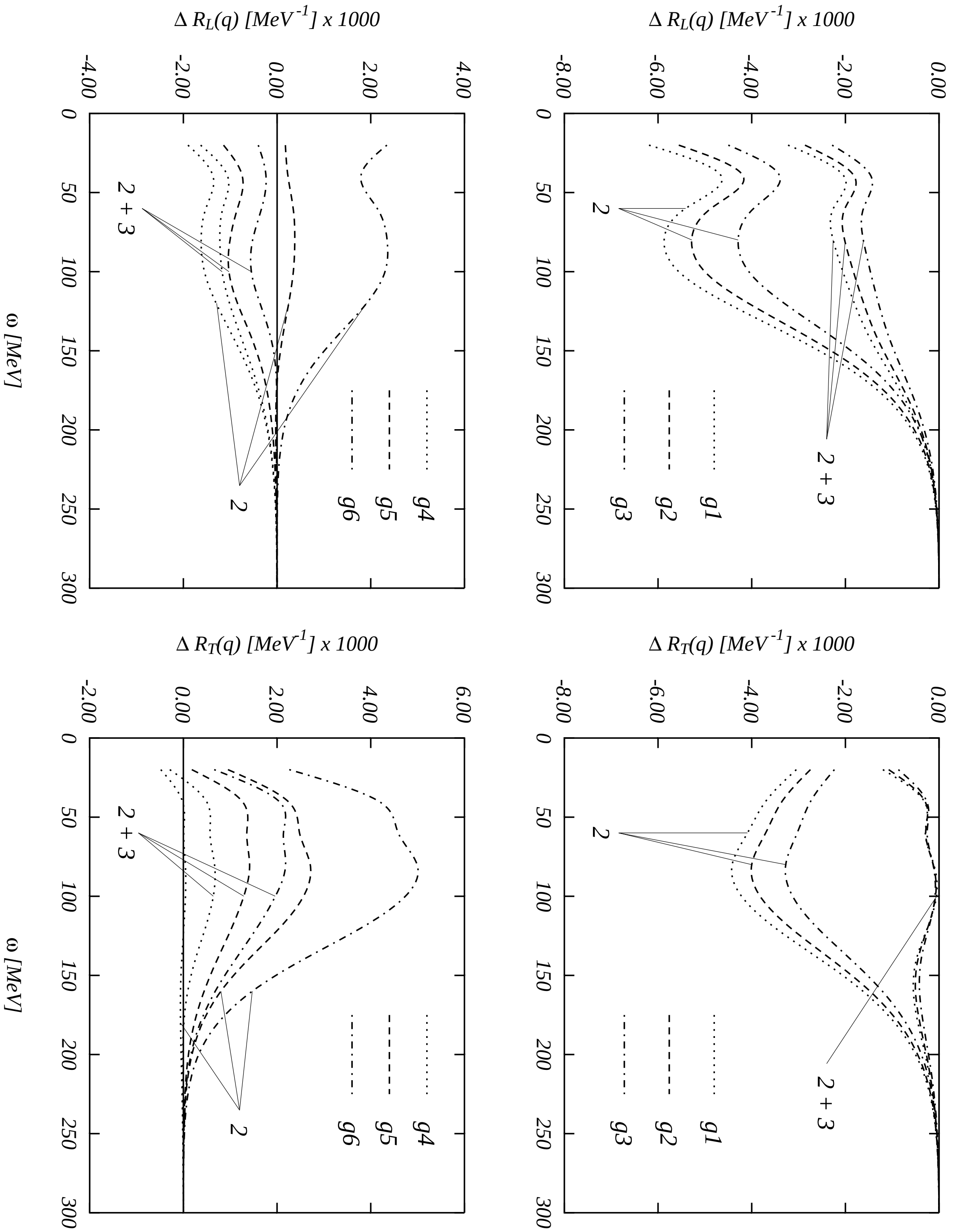

Figure 14: Differences between correlated and uncorrelated ^{16}O responses at q=400 MeV/c obtained with the S3 single particle wave functions for the correlations of Table 4. The left (right) panels refer to the longitudinal (transverse) responses. The curves labelled 2 indicate the results obtained with only the two-point diagrams of Fig. 1. The other curves have been obtained including all the diagrams.

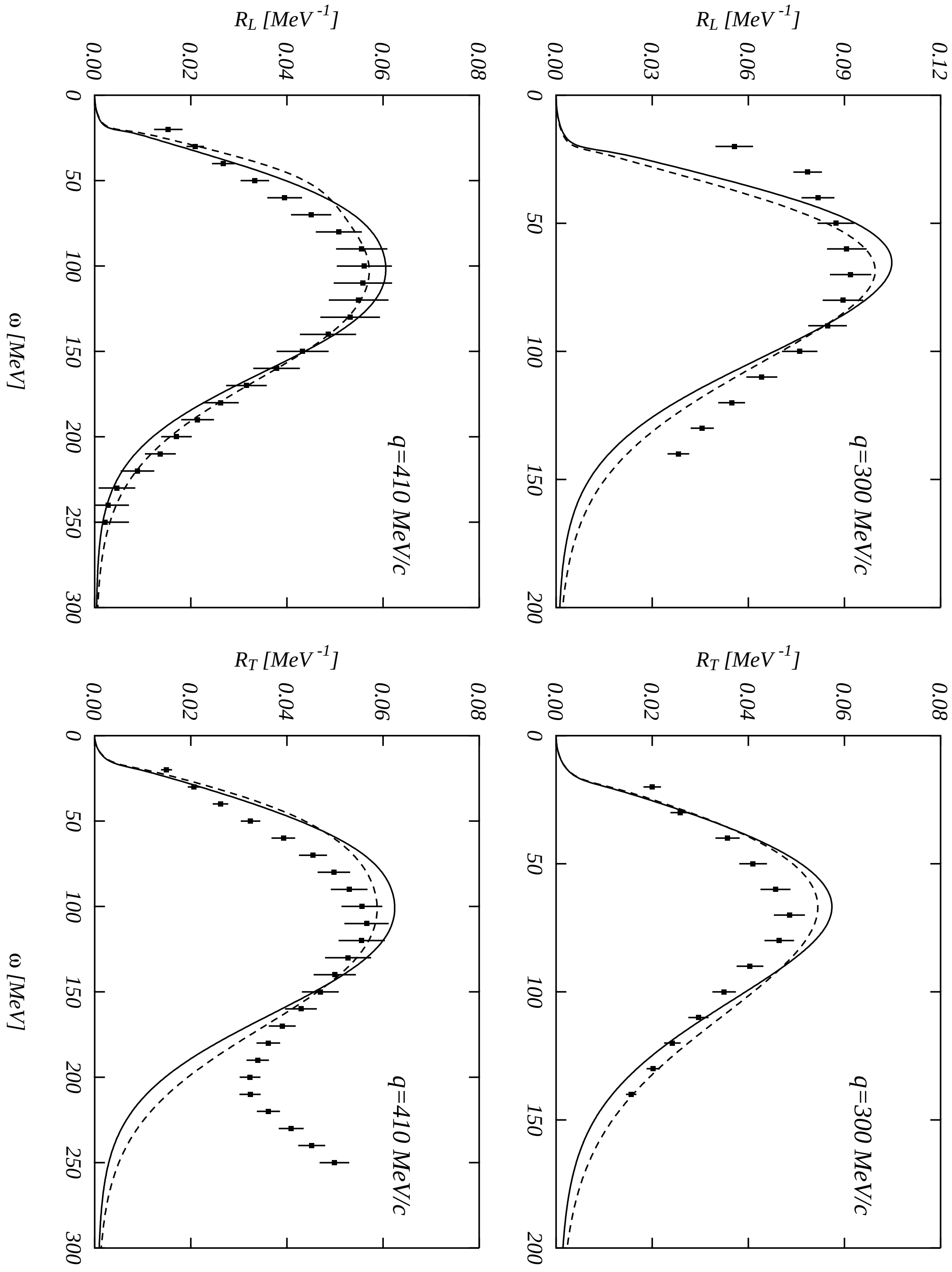

Figure 15: ^{40}Ca longitudinal and transverse responses compared with the data of Ref. [33]. The full lines are the results obtained with the V8 input while the dashed lines have been obtained with the S3 input.

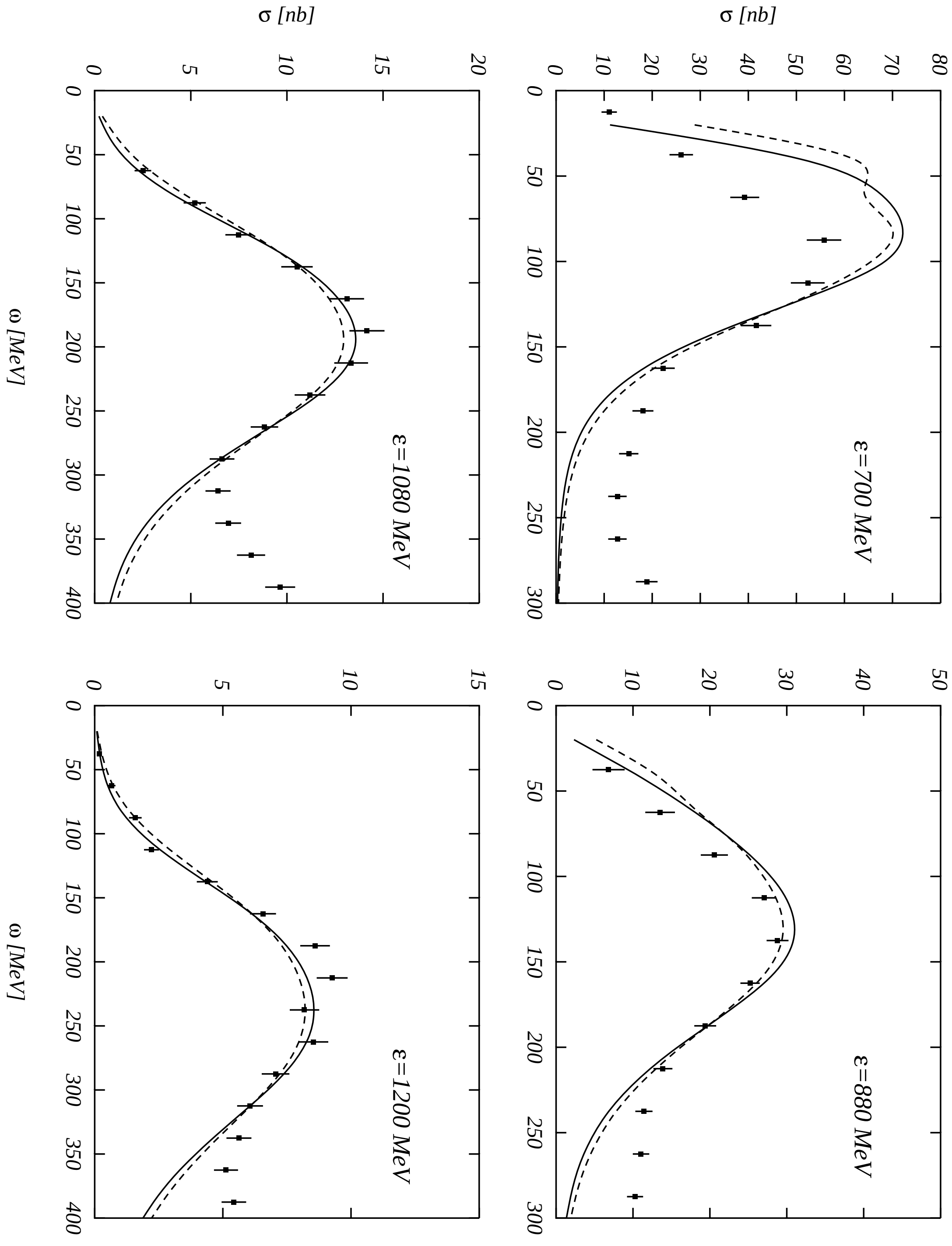

Figure 16: Electron scattering inclusive cross sections on ^{16}O for fixed scattering angle, $\theta = 32^{\mathrm{o}}$, and various values of the electron energy. The experimental data are taken from Ref. [34]. The full and dashed lines show the results obtained with V8 and S3 inputs respectively.

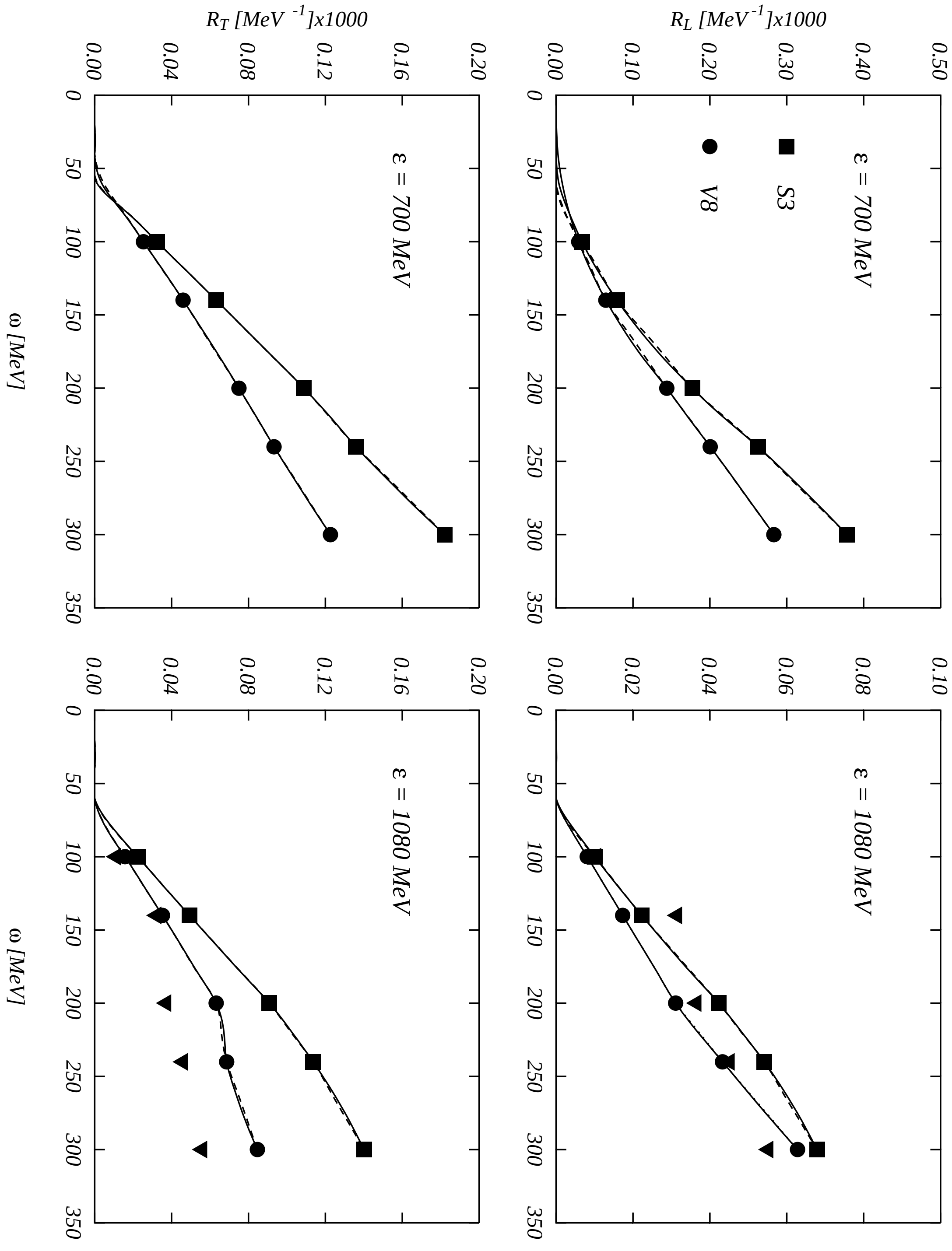

Figure 17: The symbols shows the calculated values of the longitudinal and transverse two-nucleon emission responses in ^{16}O. Squares and circles show the results obtained with the V8 and S3 input respectively. The triangles have been calculated using the V8 correlation and the S3 mean-field wave functions. The various lines have been obtained by interpolating the points with various techniques: linear (dashed lines), quadratic (full lines), cubic spline (dashed dotted).

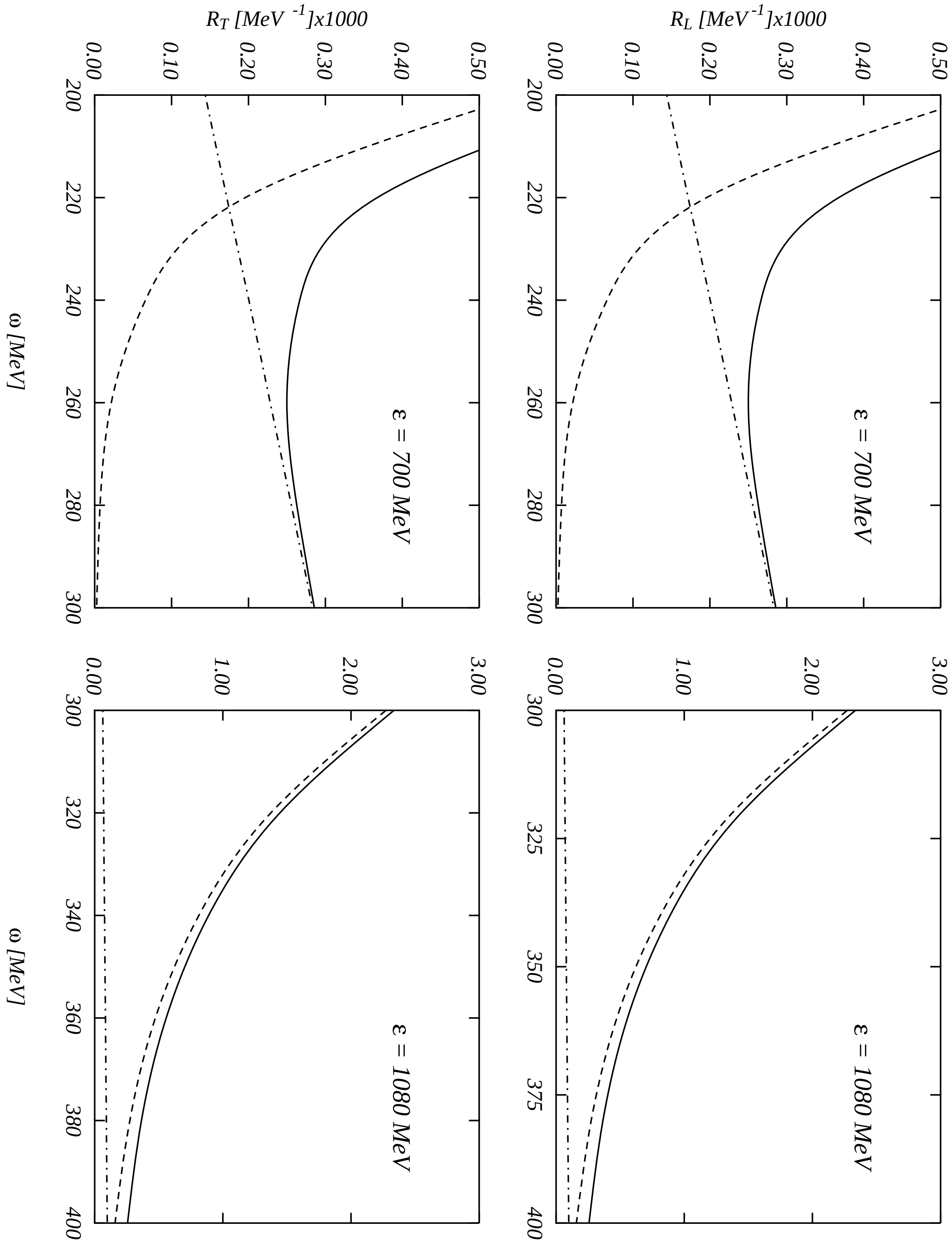

Figure 18: Longitudinal and transverse responses of ^{16}O in the dip region calculated with V8 input. The dashed lines show the 1p-1h responses, the dashed dotted lines the 2p-2h responses and the full lines show the total responses.

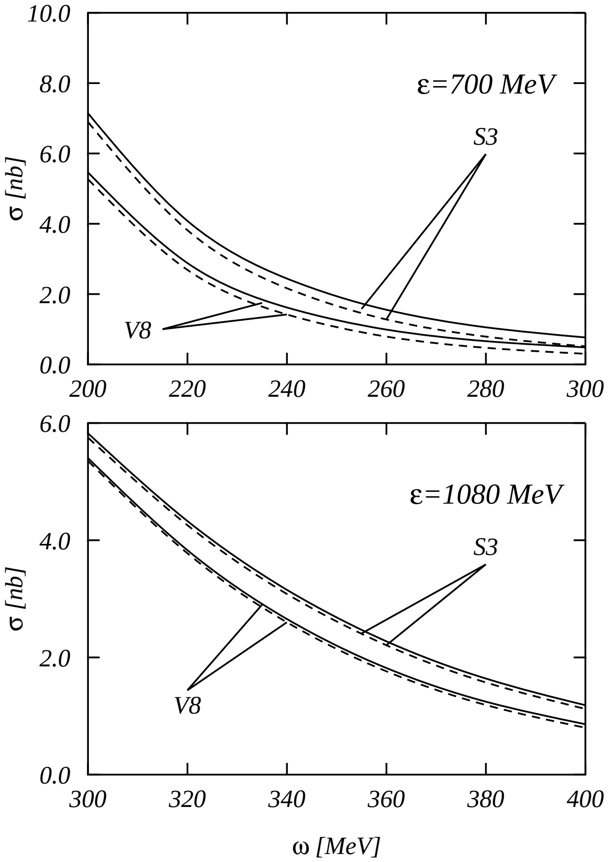

Figure 19: Inclusive cross sections on ^{16}O for two values of the electron incoming energies and a scattering angle of 32^0. The full lines have been obtained including both 1p-1h and 2p-2h contribution while the dashed lines show the 1p-1h one.